Nanoceramic Reinforced SWCNT/PVA Composites for Supercapacitors

Faiza

Registration no. # 00000117287

A thesis submitted in partial fulfillment of the requirements

for the degree of Master of Science

in

Chemistry

Supervised by: Dr. Zahida Malik

Department of Chemistry

School of Natural Sciences

National University of Sciences and Technology

H-12, Islamabad, Pakistan

2018

National University of Sciences & Technology

MS THESIS WORK

We hereby recommend that the dissertation prepared under our supervision by: FAIZA, Regn No. 0000117287 Titled: Nanoceramic Reinforced SWCNT/PVA Composites for Super Capacitors be accepted in partial fulfillment of the requirements for the award of **MS** degree.

Examination Committee Members

1. Name: PROF. HABIB NASIR   Signature: _____

2. Name: DR. AZHAR MAHMOOD   Signature: _____

3. Name: _____   Signature: _____

External Examiner: DR. GHULAM MUSTAFA   Signature: _____

Supervisor's Name: DR. ZAHIDA MALIK   Signature: _____

_____
Head of Department

01- 02 - 2018
Date

COUNTERSINGED

Date: 01/02/18

_____
Dean/Principal

THESIS ACCEPTANCE CERTIFICATE

Certified that final copy of MS thesis written by **Ms. Faiza**, (Registration No. **00000117287**), of **School of Natural Sciences** has been vetted by undersigned, found complete in all respects as per NUST statutes/regulations, is free of plagiarism, errors, and mistakes and is accepted as partial fulfillment for award of MS/M.Phil degree. It is further certified that necessary amendments as pointed out by GEC members and external examiner of the scholar have also been incorporated in the said thesis.

Signature: _____

Name of Supervisor: Dr. Zahida Malik

Date: 01.02.18

Signature (HoD): _____

Date: 01-02-2018

Signature (Dean/Principal): _____

Date: 01/02/18

Dedicated to

My Beloved Family

My Sister Aneeqa Ijaz

(may her soul rest in peace)

My Husband & Daughter

Respectful Teachers & Mentors

Helping Friends

NUST & Pakistan

Acknowledgements

Abstract

Here we present mechanical engineered effect of SWCNT nanoceramics on polymer thin films. The composite thin film synthesis with different concentrations of nanoparticles and (functionalized SWCNT) f-SWCNT (yield range 75-80%) in (Polyvinyl Alcohol) PVA matrix was carried out by "*Simple Solution Deposition Method*". Characterization was accomplished by FTIR, XRPD, SEM and AFM. FTIR results confirmed the successful functionalization of SWCNT's with bands appearance at 3213 (-OH), 1788 (-C=O), 1320 (-NO$_X$), −C-H stretch at 2136 cm^{-1} and 602 cm^{-1} (-SO$_X$). It has also confirmed the synthesis of f-SWCNT/PVA/MO by appearance of individual peaks of all constituents. Peaks of SWCNT's and polymer were also confirmed by phase analysis through XRPD analysis which not only confirmed the synthesis of f-SWCNT/PVA/MO composites but also the single phase nano NiO and CuO materials with crystallite sizes, 34.5 and 4.05nm, respectively. SEM and 3-D AFM images showed topographic image of SWCNT's using tapping mode. Transmittance was controlled by using least concentration of SWCNT and transmittance was measured by using UV-Vis spectrophotometer it was seen that transmittance and absorbance peaks were observed in ultra violet range and it was observed that least concentration of SWCNT give the highest transparency. Same trend was observed in case of metal oxides so the composite with least concentration of SWCNT and MO shows best transparency to be used in transparent super capacitors. UV-Vis DRS (Diffused Reflectance Spectroscopy) revealed band gab between 4.2-4.9 eV for composites which are more suitable for super capacitor application as compared to those of NiO (3.86 eV), CuO (3.07eV) and PVA (6.2eV) separately. Band gap of PVA reduced to 4.8 to 4.7 and 4.5 eV by increasing concentration of NiO and CuO while f-SWCNT's caused further reduction in band gap to 4.38, 4.30 and 4.20 eV. Dielectric constant, dielectric loss, tan loss and AC-conductivity was evaluated and found that all these parameters could be controlled according to need by varying concentration of MO and SWCNT's. it was seen that the composites with least concentration of MO shows best current storing ability as in case of CCP 1 value of dielectric constant, dielectric loss, tan loss and ac conductivity was 3.3 x 10^7, 9.7 x10^8, 4.5 and 19 Sm^{-1}, respectively and for CNP1 value of dielectric constant, dielectric loss, tan loss and Ac conductivity was 1.7 x 10^7, 3 x10^8, 2.5 and 9 Sm^{-1}, respectively. Physical properties of composites anticipate them good potential candidates for supercapacitor applications. The tensile strength of of f-SWCNT/PVA/MO composites got enhanced with SWCNT concentrations whereas toughness got enhanced due to MO concentration. The elasticity of metal oxides was enhanced by presence of PVA from as calculated Young's modulus of PVA was 71.2 Pa. For simple PVA/CuO values of Young's modulus were 8.2, 18.9 and 27.2 Pa and were enhanced to 62.4, 22.5 and 57.7 by addition of f-SWCNT's. Similarly for PVA/NiO values of Young's modulus were 22.7, 25.7, and 30.9 Pa by addition of f-SWCNT's enhanced to 28.3, 31.3 59.0 Pa.

Table of Contents

List of Figures

List of Table

Abbrivations

AFM	Atomic Force Microscopy
CL	Cathode Luminescence
CNT	Carbon nanotubes
CV	Cyclic Voltametry
DRS	Diffused Reflactancec Spectroscopy
EDLC	Electric Double Layer Capacitor
EIS	Electron Impedence Spectroscopy
PVA	Poly Vinyl Alcohol
FTIR	Fourier Transform Infrared
f-SWCNT	Functionalised Carbon Nanotube
HRTEM	High Resolution Transmission Electron Microscopy
IR	Infrared
MO	Metal Oxide
MWCNTs	Multi Walled Carbon nanotubes
SEM	Scanning Electron Microscopy
SWCNT	Single Walled Carbon Nanotubes
TEM	Transmission Electron Microscope
UV	Ultra Vilot
XRPD	X-ray Powder Difraction

Chapter 1

Introduction

1.1. Nanochemistry

Nanochemistry is basically a related to solid state chemistry in which a chemist focuses on preparing as possible as little piece of matter having nanometer size in one, two and three dimensions [1]. The nanomaterials exhibit different chemical and physical properties as compared to bulk counter parts bulk materials. Nanomaterial could be used in quantum electronic, chemo selective sensing, photonics, nonlinear optics and information storage and processing [2].

1.1.1. Classification of nanomaterials

Nanomaterials could be classified on different basis as discussed below:

1.1.1.1. On basis of origin. On the basis of origin, nanomaterial could be classified into two following classes.

a. Natural Nanomaterials: The nanomaterials that are obtained from natural resources or exist naturally for example viruses, proteins and lotus leaf. Some natural colloids are like blood and milk, few are of aerosol type, like fog and few are of gel type, like gelatin.

b. Artificial Nanomaterials: Materials that are prepared by fabrication chemical or physical processes for example carbon nanotube, carbon nanoparticles like quantum dots.

1.1.1.2. On basis of dimension. On basis of dimension nanomaterials are classified into following classes:

a. Zero dimensional (0-D): The nanomaterials that have no dimension out of nanometer range. Its only property is its location for example quantum dots and nanoparticles they are mostly spherical, and their diameter lies in the range 1-50 nm. Their cube and polygon shape could also exist.

b. One dimensional (1-D): In these materials one dimension is out of nanometer range it includes nano wires, nano rods and nanotubes. Their length could be of several micrometers but their diameter lies in nanometer range.

c. Two dimensional (2-D): In these materials two dimensions are out of bound of nanometer range for example nano film, nano sheets and nano wells their thickness lies in nanometer range**.**

d. Three dimensional (3-D): Their all three dimensions are out of nanometer range it include bulk material although their individual building blocks are in nanometer range (1-100 nm) [3] [4].

1.1.1.3. On basis of structural configuration. Based on structural configuration nanomaterials have four classes as discussed below.

a. ***Carbon based nanomaterials:*** They could be ellipsoidal, hollow or tubes. For example; fullerenes are ellipsoidal, and nanotubes are cylindrical. The main component of these material is carbon.

b. ***Metal based nanomaterials:*** The main component of these material is metal like Nano gold, Nano silver and metal oxides like titanium dioxide and closely packed semiconductors like quantum dots.

c. ***Dendrimers:*** Dendrimers are actually the polymers which are of nanometer size on their surface there are so many chain ends which could be used for catalysis. They also have internal cavities in which new species could be carried and this property could be used for drug delivery.

d. ***Composites:*** In these different nanomaterials are combined to enhance their thermal, electrical, flame retardant and mechanical properties [5] [6].

1.2.   Carbon nanotubes

Fullerenes were discovered in 1980s by Buckminster Fullerene a few year later in 1990's this discovery led to the synthesis of carbon nanotubes (CNTs), these CNTs attracted the interest of researchers due to having remarkable electrical, thermal and mechanical properties. The reported strength of CNTs is 10-100 times greater than steel, elastic modulus is greater than 1 TPa as compare to diamond (elastic modulus 1.2 TPa). Exceptionally, CNT's are thermally stable up to 2800°C in vacuum that is twice higher than that of diamond and have current carrying capacity 1000 times greater than copper wires.

1.2.1. Atomic Structure and Morphology. The graphene sheets (2-D) are rolled and form cylindrical structure of carbon nanotubes having three neighboring carbons Carbon nanotubes were first synthesize by Iijima *et al*. Different methods for the synthesis could be used like arc discharge, laser ablation, gas phase catalytic growth, and chemical vapor deposition method

[7]. The physical and chemical properties greatly depend upon morphology; diameter and length. Mainly, CNTs exist either as single walled CNTs (SWCNTs) or multiwall CNTs (MWCNTs). The structure of CNTs could be described by chiral vector C_h and chiral angle (θ) where chiral angle determines the amount of twist in chain.

Chiral vector is related to other parameters by following formule,

$$C_h = na_1 + ma_2$$

Where, a_1, a_2 are unit vectors and m, n are integers that show number of steps along zigzag carbon bond.

1.2.2. Carbon nanotubes thin films. The transparency of CNTs is more than 90% which makes them useful as transparent electrodes and sensors. The major challenges encountered while working with CNTS are; homogeneous dispersion, synthesis cost and purification of CNT's [8]. CNT's thin films could be prepared by different methods; plasma enhanced chemical vapor deposition [9], solution based deposition and spin spraying method, etc.

1.2.2.1. Properties of CNT thin films. The properties of individual CNTs are studied extensively. In thin films, the properties of individual tubes are also enhanced by tube-tube interaction.

a. Transport properties: SWCNTs have very much high mobility $> 100,000$ cm^2/vs. they also occupy high current carrying capacity. The resistance of carbon nanotubes depends upon their length CNT' of 500 nm length have resistance of 6-7 kΩ. In conclusions you insisted that SWCNTs are semiconductor in nature.

b. Electronic and Optoelectronic properties: The band structure of individual CNT's has been widely explored. The electronic structure basically depends upon the wrapping of graphene sheets. By doping with Boron and Nitrogen leads to p-type or N-type semiconducting behavior of tubes [10].

c. Transmittance: The films of carbon nanotubes show transmittance and electrical conductivity if its thickness is 10-100 nm. The transparency depends upon tubes purity, length, and film thickness and dispersion quality. The film transparency losses with increasing length.

1.3. Characterization Techniques
Following techniques were employed to characterize the thin film samples.

1.3.1. Foriour Transform Infrared-Spectroscopy. IR spectroscopy is the technique that operate at ambient temperature at analytical level. And it monitors the vibrations of functional

group directly that characterize the molecule. It provides continuous operation and it comprises low maintenance. It usually ranges from 0.7 µm to 1000 µm. Mid-IR is not very much used widespread now a days as near IR gives more precise bands. In near-IR the bands are mostly weak and tend to show more overlapping [11] [12]. FT-IR is usually used to get information like; characterization of unknown compounds, quality or consistency of sample and amount of component in mixture. When IR radiations passed through the sample some radiations get transmitted and some of them are absorbed as a result of that spectrum is obtained. Fig 1.1 shows the working principle of FTIR spectroscopy.
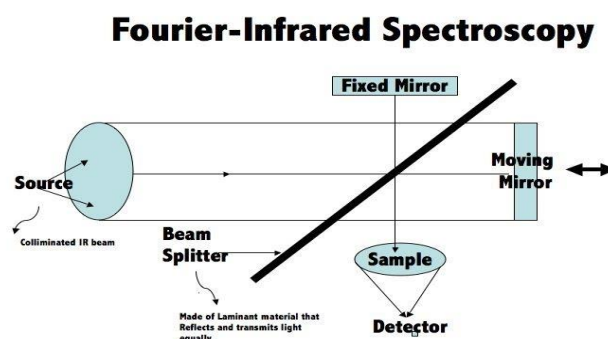
Figure 1.1. Construction of IR Instrument [11]

1.3.1.1. Selection rule. In an IR active material there must be some structural components with dipole moment change during vibration to show infrared absorption. It occurs in *heteronuclear* molecule when it contracts or expands.

1.3.1.2. Factors cause broadening. It usually shows broad bands due to numerous different factors, one is *Doppler's Effect*. As radiation move towards or away from the observer frequency shifted due to which broadening occurs. Another factor that involved in broadening is *Heisenberg's Principle*, when atoms collide with each other having finite life time of excitation. The energy of transition is uncertain as average life time of excitation of atoms is 10^8 s. They some time show transition in energy state when come back from high energy state due to which broding occur. The relationship exist between excitation life time and band width of absorption. it has direct relation with each other [13].

1.3.1.3. Modes of vibrations. The absorption of energy depends upon modes of vibrations that takes place in a molecule due to change in its dipole moment the vibration could be in plane or out of plane,

4

- In Plane can be either Scissoring or Rocking

- Out of Plane can be either Wagging or Twisting
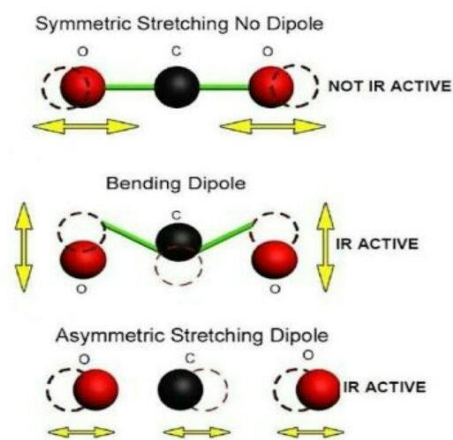
Figure 1.2. Vibrational modes of IR active bonds [14]

Ranges of absorption of different functional groups are given in figure 1.3.
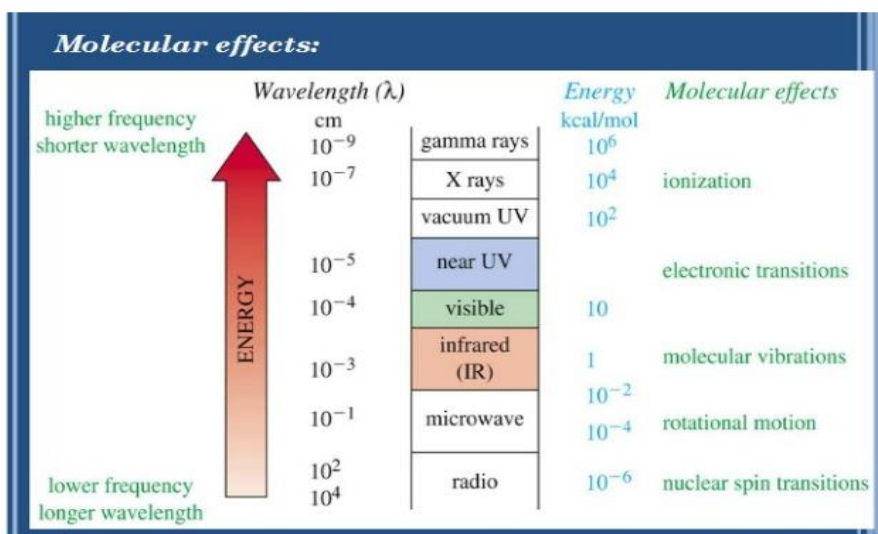
Figure 1.3. Different frequency ranges [15]

Figure 1.4 Indicates different symmetrical and unsymmetrical vibrational modes
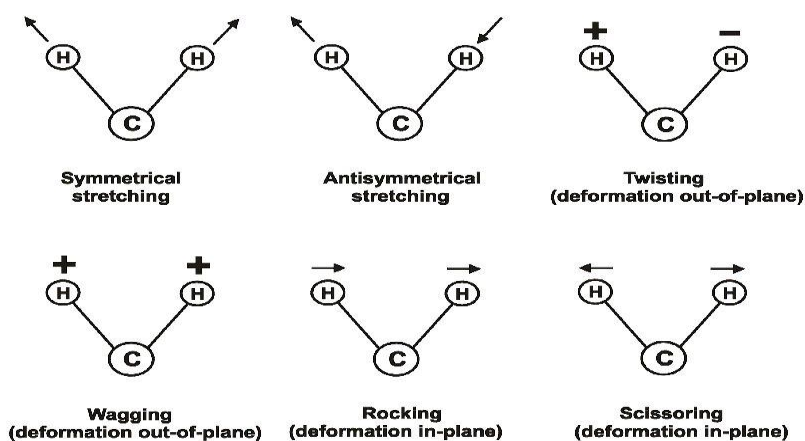
Figure 1.4. Modes of vibrations [16]

1.3.1.4. Degree of freedom. In diatomic molecules there is three degrees of freedom in translational motion and two degrees of rotational motion. The atoms in diatomic molecule also move with respect to each other. Polyatomic molecule having N no of atoms have 3N degree of freedom. An atom could have different bending and stretching vibrations. The vibrations could be symmetrical or asymmetric [13]. The energies with these vibrations are quantized and specific vibrations are allowed principle of modes can be seen through figure 1.5.

Figure 1.5. Principle of modes [17]

1.3.1.5. Complicating Factors. To interpret IR spectra there are few factors that make it complicated. Sometimes analogous or multiples of the absorption peaks appear that are called as *overtones. Combination bands* also occurs. Another factor is *Fermi Resonance*. When two

absorptions are so close to each other or two peaks appear when one peak is expected fermi resonance occurs. Sometimes a single peak is divided into two or combination band occur at same frequency of fundamental frequency or sometime mismatch frequencies that differ with few wave numbers. The two bands are known as *Fermi Doublets*. Mostly *coupling* occur mostly due to carbon backbone and present of oxygen and nitrogen. In coupling energy level mixing occur and same vibrational modes resulted.it mostly occurs if frequencies of adjacent bonds are similar. In this case it become difficult to assign same band to a specific bond [13] [15].Over tones of different groups is give in figure 1.6.
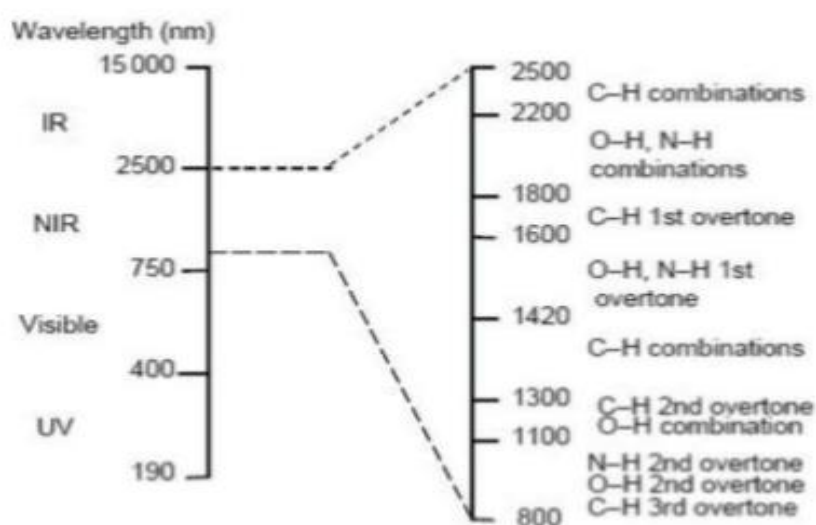
Figure 1.6. Overtone range [7]

1.3.1.6. FT-IR Spectrometers. In FT-IR spectrometers the main part is amplitude division interferometer. The main construction of spectrometers is still according to the Michelson design [11] [18]. It mostly consists of; Beam splitter, compensating plates and pair of mirrors. Mostly organic compounds absorb in the range 4000 cm^{-1} to 400 cm^{-1}. Important regions are 1650 cm^{-1} onward and other part is finger print region it is not very useful to characterize unknown compounds. Energy levels of different molecules show different transitions according to the same equation,

$$\overline{n} = \frac{1}{2pc}\sqrt{\frac{k}{m}}$$

Where

7

$$m = \frac{m_1 m_2}{m_1 + m_2}$$

k is the force constant, m is the reduced mass. Greater the mass of the molecule slower will be its vibration. k and bond strength are proportional to each other. Sometime in the absence of O-H group a small peak is observed at 3450 cm^{-1} that is overtone of C=O vibration. IR peak is as strong as dipole moment change is greater during vibration. Vibrational modes of coupling bond could be symmetric or asymmetric. Symmetric stretch requires higher energy and asymmetric stretch requires low energy [19] [15] [18].

Strategy to interpret spectra. First of all by using molecular formula evaluate the units of unsaturation. Divide the spectra into three parts,

1. X-H region
2. Sp region
3. Double bond region
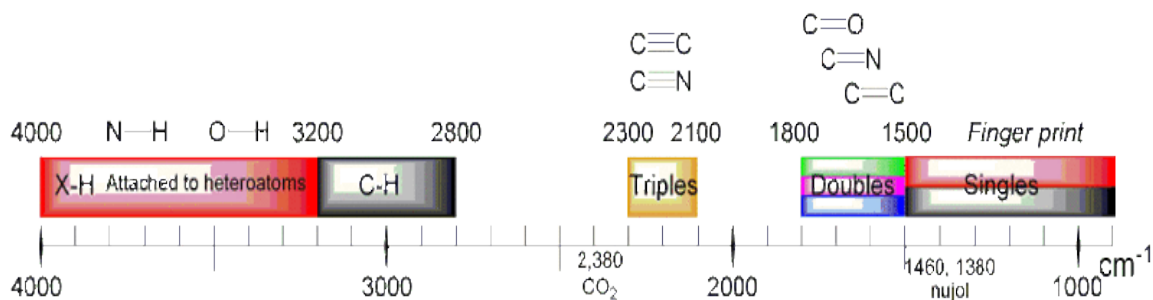
Figure 1.7. Absorbance range of different group [7]

- Analyze the spectrum from to right to left and if a strong and broad band observed at 3500 cm^{-1} it represents presence of OH.
- If weak peaks are observed in this area than amines (N—H stretch) are indicated. 3000 cm^{-1} C—H aliphatic stretches are observed to the right
- C—H of alkenes & aromatics are at left. Aldehyde and ketones C—H stretch show peak at ~ 2720 cm^{-1}. Area from 1820 to 1630 cm^{-1} analyzed where strong peaks of C=O observed which is strongest peak in the spectra.
- The region from 1250 to 1000 cm^{-1} are the C—O stretches of ethers, esters and acids [12] [20] [18].

1.3.2. X-Ray Powder Diffraction. X-ray powder diffraction is an analytical tool used for qualitative and quantitative analysis of crystalline materials. It provides information about

phase distribution, crystallite size, degree of crystallinity, geometry, epitaxy and lattice parameters etc.

Basic principle that is employed in X-ray diffraction technique is interference of the X-ray radiation that is constructive and diffracted by the crystalline materials, could be explained by Bragg's Law. By this law X-ray reflected when fall at surface of a compound, travels less distance as compare to the X-ray that reflected from a plane of atoms that are present inside the crystal. X-ray penetrate and travels down to the lower layers, reflected and scattered back over the same distance before coming back to the upper layer. The distance travelled by X-rays depends on the separation of the layers and the angle with which X-ray entered the substance surface. Diffraction takes place only when the distance covered by the parallel X-rays is an integer multiple of the wavelength. Braggs law could be written in form equation given below:

$$n\lambda = 2dSin\theta$$

Where n is an integer having whole number value of interference, λ is a wavelength of the incident radiation, θ is an angle between the incident ray and crystal layers while d is the interspacing present between the layers. Structural information of crystal lattice can be determined by monochromatic radiation beam that is focused on compound, In cathode ray tube basically poly chromatic rays are produced than these polychromatic rays pass through monochromator that produce monochromatic rays that are placed onto atomic planes. The transmitted, scattered and refracted rays generate the spectra containing peaks of different intensities. Construction and working of an XRD spectrometer is give in figure 1.8.

1.3.2.1. Uses and Applications of XRPD. XRPD is a non-destructive technique which efficiently determines the crystal structure, crystallite size, phases present in the sample, atomic arrangement, lattice parameters and many other properties of the material. It is used in almost all the fields due to its versatility and accuracy in giving maximum structural information about the sample.
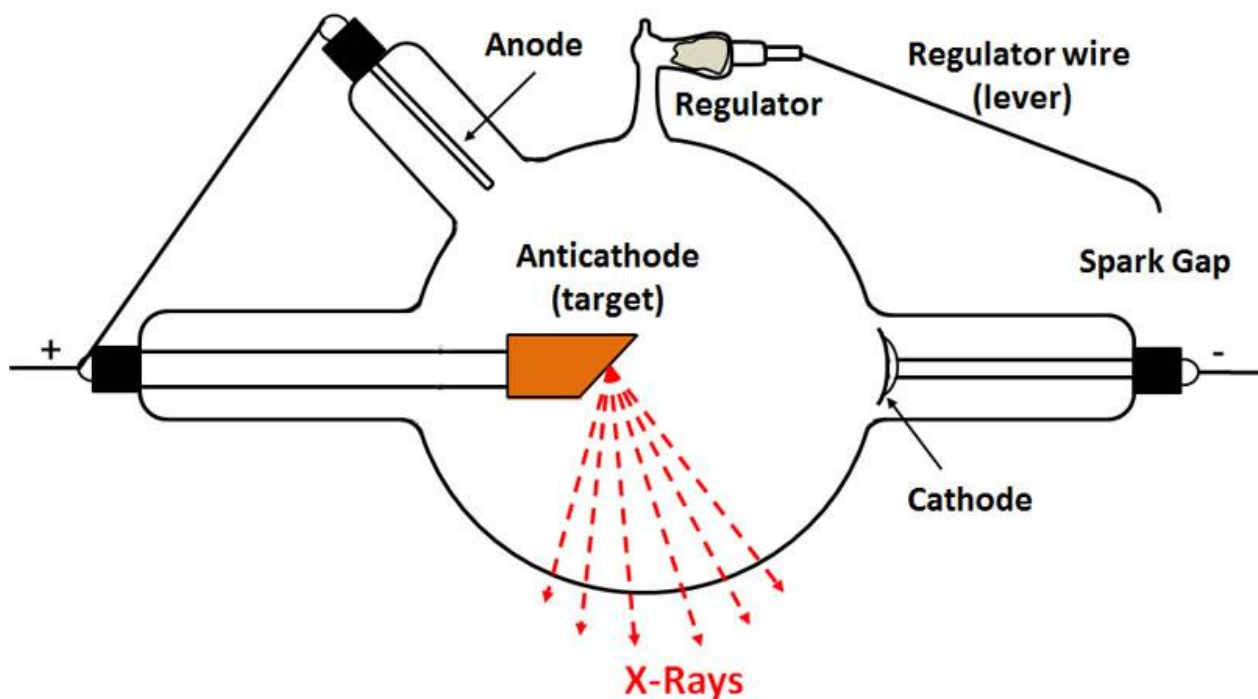
Figure 1.8. Working of X-ray spectrometer

1.3.3. Scanning Electron Microscopy (SEM). The scanning electron microscopy (SEM) is used to focus the surface of sample by using electron beam. The information of the sample structure and topography is obtained as beam of electrons interact with sample and various signals are generated sample could be analyzed at elevated temperatures and resolution up to 1 nm could be achieved. A very small amount of the sample is used for this purpose solution form of sample could also be analyzed. SEM image could be obtained by back scattered or secondary emitted electrons. The secondary emitted electrons are collected and by detector image is formed. [14]. First of all SEM was introduced by McMullan [21] and first microscope was prepared by Manfred von Ardenne [22] [23].

1.3.3.1. Principle. The beam of electrons is generated, and it interact with the atoms at different depths and various signals of different types are generated which are given as follows:

- Secondary electrons (SE)
- Cathode luminescence (CL)
- Backscattered or reflected electrons (BSE)
- Transmitted electrons
- Specimen current
- Characteristic X-rays

10

But all these signals could not be detected by single machine. Secondary emitted electrons emitted from surface of the sample and resolution till 1 nm could be attained. While in case of backscattered electrons the electrons emitted from the depth of sample [24]. Different types of ejected radiations are mentioned in figure 1.9.
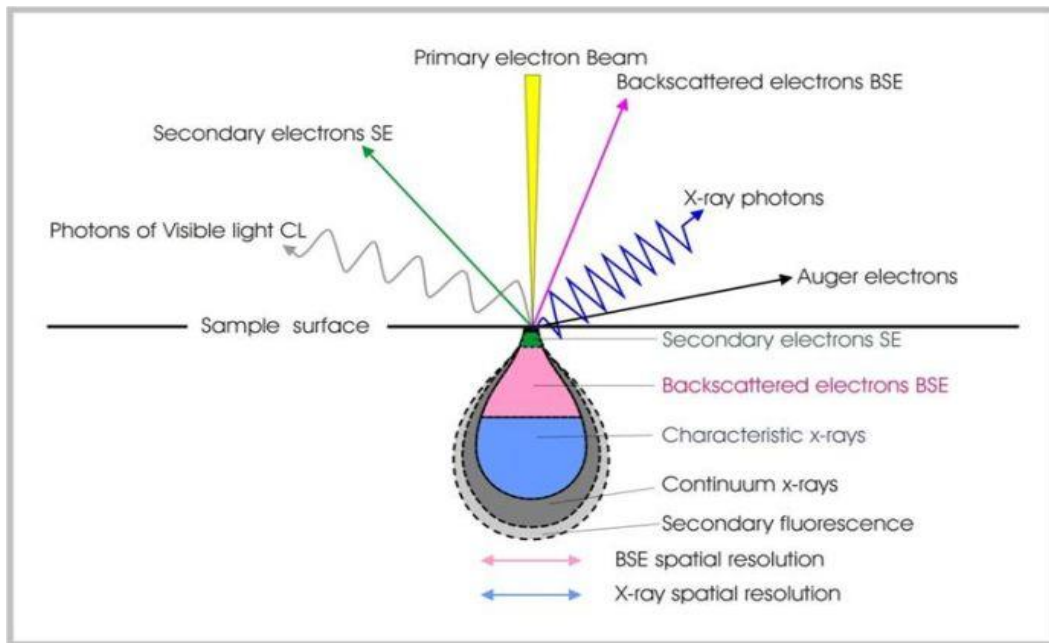
Figure 1.9. Different types of radiations emitted from SEM [25]

BSE can detect image up to 10 to 15 nm. When electron beam ejects the electrons from inner shell of the sample and electron from high energy come to fill its place than characteristic X-rays are produced which are of high energy and provide information about elemental composition. Its magnification can vary from 10 times to more than 50000 times [26].

1.3.3.2. Sample Preparation. For SEM sample should be prepared according to following aspects the sample should be: conductive, appropriate size of specimen gage and should be able to withstand under vacuum conditions. It is necessary to coat the nonconductive sample usually with gold, platinum, carbon, tungsten, chromium or osmium [24] [21]. Figure 1.10 displayed the sample holder for SEM analysis, the samples are placed on these stubs of specific dimensions.
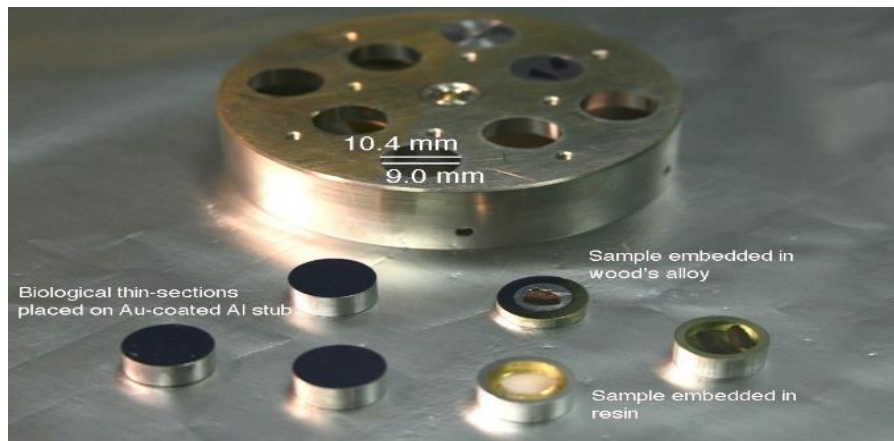
Figure 1.10. SEM stubs used to analyze the sample[27, 28]

1.3.3.3. Scanning process. Tungsten (electron gun) is useful due to its high melting point and it has lowest vapor pressure as compared to the metals and it is not very much expensive. Through this electron gun electron beam is emitted and is focused by two condenser lenses. The energy of electron beam ranges from 0.4 keV to 40 keV. The beam is focused at a point whose diameter is 0.4 to 5 nm. Than beam passes through a column where deflector plates are present where final lens is present that focus the beam at rectangular surface of the sample [29] [30].

Construction of SEM is given in figure 1.11, the electron beam interacts with sample surface and primary electrons are emitted after that different scattering transmission and ejection of electrons occur, the obtained signals amplifies by amplifier, synchronized with system and converted into the digital image. Magnification in SEM is not due to the lenses they are present only to focus the beam of electron not to magnify the image. It is actually related to the dimensions. Greater will be magnification if the raster size of the specimen reduced.it means that current supplied can control the magnification [31] [32].
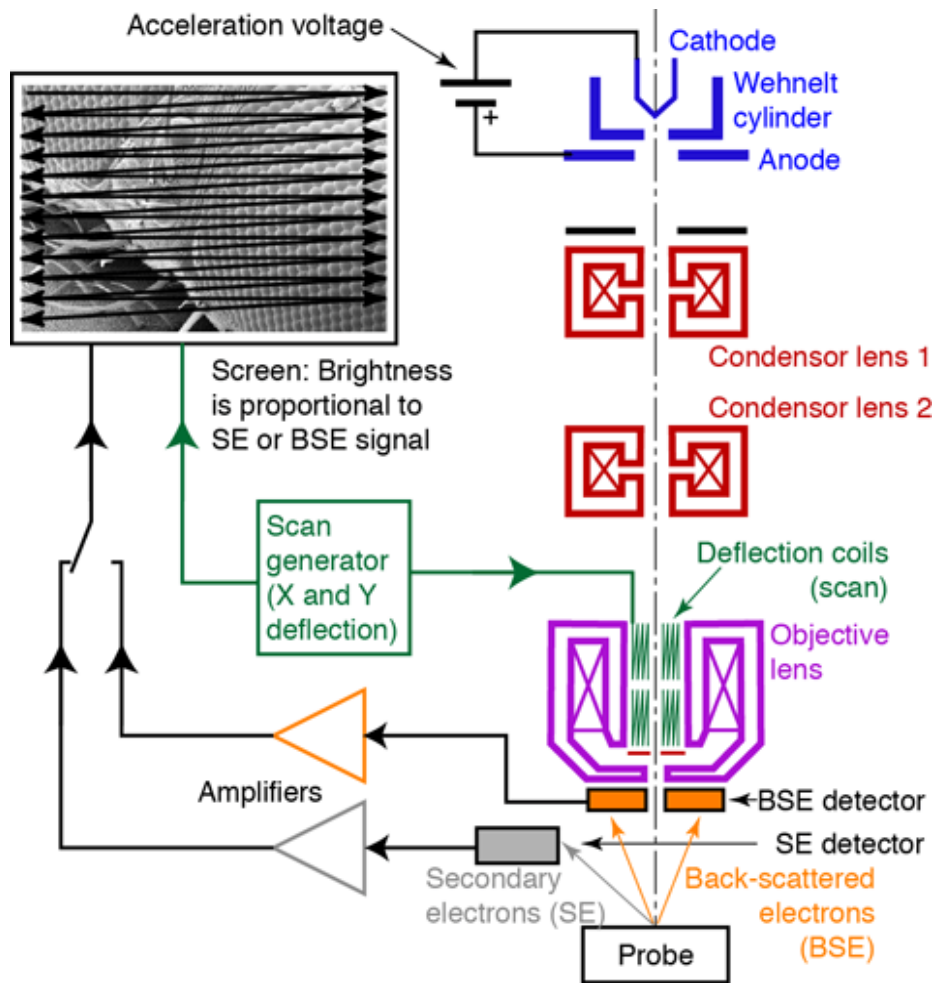
Figure 1.11. Instrumentation of the SEM [33, 34]

1.3.4. Atomic Force Spectroscopy.

Atomic force microscopy is a type of scanning probe microscopy that shows high resolution on fraction of nanometer. It mainly uses mechanical probe that touches or feels the surface and gives the image of surface. It provides very precise scanning. It mainly provides following informations,

1.3.4.1. Force measurement. In mode of measurement, force between probe and sample is measured in order to their mutual separation. Depending upon the separation of probe and sample the adhesion between both is measured that gives the information about adhesion property of sample. As cantilever come closer to the surface attractive forces of tip deflect cantilever toward surface and further reduction in distance causes repulsion that deflects cantilever away from the surface in this way force between cantilever tip and sample can be measured

1.3.4.2 Imaging. In it high resolution of surface is obtained it tells about dimensional topography of the sample. Cantilever interact with surface of material. Cantilever scanned over region whose topography is required Feed back loop is used to control the height of the tip above the surface, thus it maintain a constant laser position so that the AFM can generate an accurate topographic map of the surface features. The tip of AFM is scanned across the sample surface along x, y direction. Cantilever deflection act as input and its output control the distance of z-axis. When the tip is in the contact with the surface of the sample the height varies and deflection of cantilever takes place. Than feedback adjust the height to the restore point. During the process AFM force remains constant.

1.3.4.3. Manipulation. Different prproperties can be measured using force measurement the values could be manipulated in following parameters:

- Stiffness
- Adhesion strength
- Conductivity

1.3.4.4. AFM Construction. The AFM instrument consists of a cantilever, support for cantilever, piezoelectric element, detection of deflection and motion of cantilever, xyz drive, stage.

1.4.   Optical properties

Optical properties were measured by using simple single beam UV-Vis Spectrophotometer and UV-Vis Diffused Reflectance Spectrometer. In next section UV-Vis DRS has been explained in detail.

1.4.1. U-Visible Diffused Reflectance Spectroscopy. UV-visible and UV-DRS spectroscopy both are used for band gap calculations. UV-visible refers to absorption spectroscopy and transmission is also measured in this technique whereas in DRS-UV reflectance is measured. Reflectance is actually the ratio between reflected radiant reflux and the incident radiant reflux (power) the term "Reflectance" was introduced by a scientist Kubelka Munk. The range of reflectance lies within 250-950 nm. Reflectance of drug, solid and rough films could be measured by DRS-UV spectroscopy. Basically two types of reflectance takes place [7] as shown in figure 1.12.
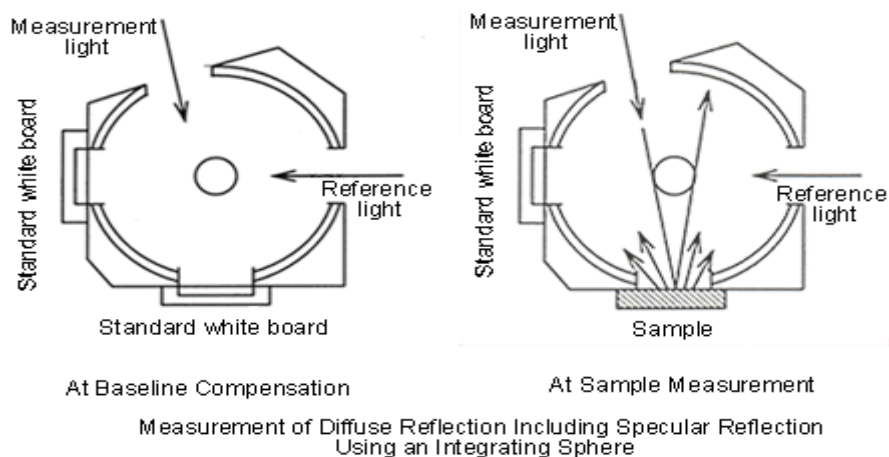
Figure 1.12. Working of UV-DRS

1.4.2. Specular reflectance & its uses. The surface that have defined angle of reflection like mirror shows specular reflectance. This type of reflection is used for films and coating e.g. polymer coating and food containers, specular reflectance is shown in figure 1.13.
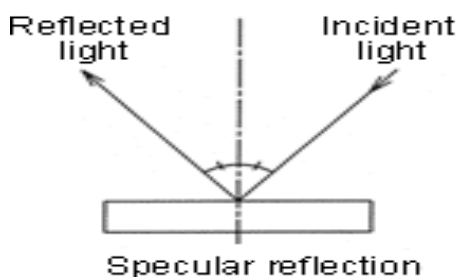
Figure 1.13. Specular reflactance

1.4.3. Diffused reflectance & its uses. Surfaces that don't have well defined angle of reflectance. In it reflected radiant energy transmit, absorb and scattered by the surface. A schematic description of diffused reflectance is shown in figure 1.14. This type of reflectance is used for strongly absorbing substances like coal, plastic and drugs.

15
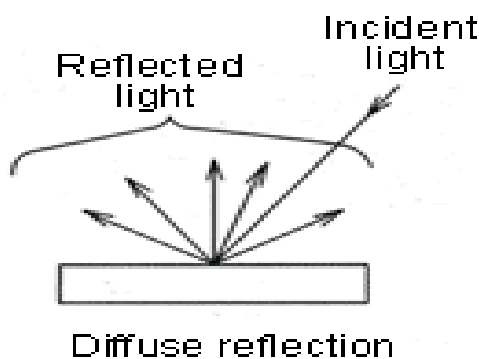
Figure 1.14. Diffused reflectance

1.4.4. Components of UV DR Spectrometer. UV-DRS spectroscopy consist of light source, integrating sphere, sample holder, detector,

Integrating sphere is used to collect the electromagnetic radiations.it is also known as Ulbricht sphere. It is optical component and contains hollow spherical cavity that has interior white coating. Small holes for entrance and exit are present. Different coating material that are used for coating; MgO, $BaSO_4$ and PTFE (Poly tetraflouroecetylene). Sample holders can either be of Centre mount cuvette style or of clip and jaw style. Most commonly used detector is photo multiplier tube which works on principle of photoelectric effect, secondary emission of electrons.

1.4.5. Principle. When light enters the sphere, many reflections diffused into highly reflective walls of the sphere. The light that is trapped on the walls of cavity of sphere dissipate in three ways. Most of light absorbs on the walls, Some light exists through the holes, Small portion strikes the detector. A steady state radiant flux is established, and it remains till the source remain active. The geometry under which measurements are performed is 0%d due to fixed 0° angle of incident for cuvette. The specular part of reflections subjected out of sphere through transmittance hole. Sample should be in sheet configuration and should be enough to accommodate the beam. For large and bulky samples jaw type holder is better. The sample should be opaque or absorbent backing must be applied. Sample holder do not transmit the light [35].Schematic illustration of it's working is given in figure 1.15.
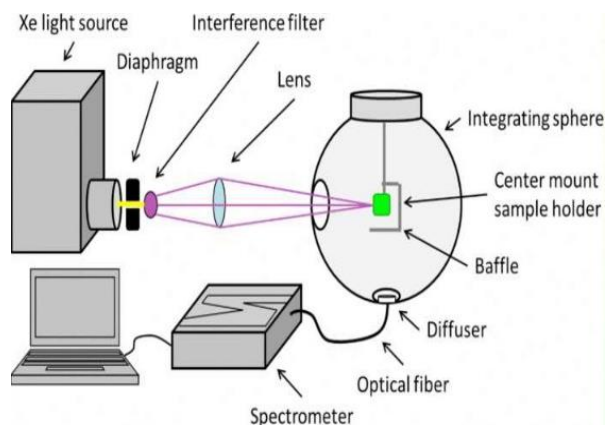
Figure 1.15. Instrumentation of UV-DRS

Tauc plot. In UV-DRS the graph is plotted against percentage reflectance and wavelength.100 % R implies that sample reflect 100% of UV wavelengths of light that interact with it. Graph between energy and $Eg(F(R))^2$ is also plotted. E_g is calculated by Kubelka Munk equation,

$$F(R) = (1-R)\ 2/2R=K/S$$
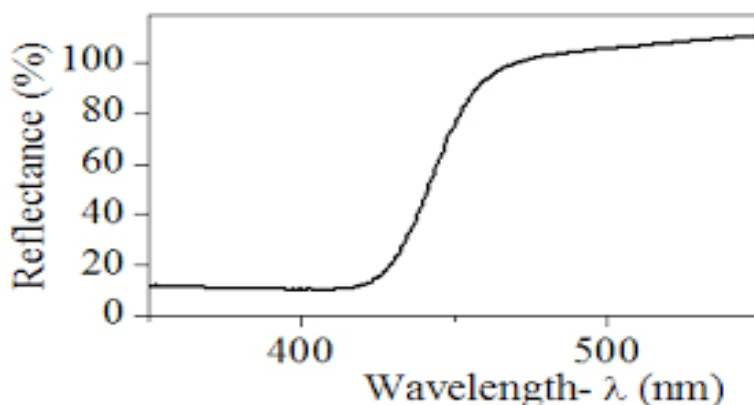
Figure 1.16 . General reflectance spectra

1.4.6. Factor affecting the reflectance. Different factors that affect the reflectance of the sample are given as follow,

- Particle size. The small particle size gives the improved spectra. The size should be 50 µm or less.
- Refractive index. The spectra of highly reflected components will be more distorted due to specular reflectance component. This effect could be reduced by sample dilution.
- Homogeneity. The sample for diffusivity measurement should be homogenous and well mixed otherwise sample is difficult to quantify.
- Packing. The sample should be loosely and evenly packed with min depth of 1.5 mm.

17

1.5.   Dielectric Properties

Dielectric properties were measured by using LCR meter,

1.5.1. LCR Meter. LCR meter name is given due to its ability to measure Inductance (L), Capacitance (C) and Resistance (R) of electronic devices.

1.5.2. Construction and Working of LCR meter. There are many techniques used for LCR meters; Wheatstone bridge and current voltage measurement. The bridge method can be used for measuring lower frequencies up to 100 kHz. A bridge is used in this method that is balanced so that at the balance point the bridge components can determine the value of component under test. Wheatstone bridge configuration is used for the analysis in which the device under test (DUT) is placed in a bridge circuit. The impedance of DUT is represented by Z_U in the circuit while the impedance of Z_1 is changeable until no current flows through Z_U whereas, the impedance values of Z_2 and Z_3 are known. The oscillator circuit operates at frequencies that can be selected before the test and it normally lowers down up to 100 kHz. This is the balance position of the bridge i.e. all the four impedances obey the equation:

$$\frac{Z_U}{Z_1} = \frac{Z_3}{Z_2}$$

Hence the impedance of DUT can be determined by using equation:

$$Z_U = \frac{Z_3}{Z_2} Z_1$$
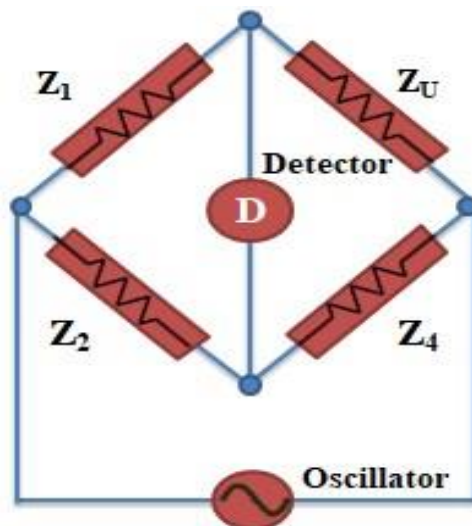
Figure 1.17. Circuit diagram for Wheatstone bridge method.

The other method is Current-Voltage measurement that is employed for applications of higher frequency. It is a precise measurement technique that can be operated at wide range of frequencies. In this technique, the current and voltage are measured for which two types of voltmeter and ammeter arrangements are used; one is for low impedance while the other is for high impedance. A phase sensitive detector is employed to make the measurements and the impedance can be found in term of inductance, capacitance and resistance through relative phase of current and voltage. These values are separately shown at the screen.

1.5.3. Uses and Applications of LCR meter. LCR meter is used to find quality factor, dissipation factor, tan loss (tanδ), and dielectric properties of the material.

1.6. Mechanical properties

For measurement of mechanical strength different machines are used most popular is universal testing machine it could test the material in: compression, bending and tension.

1.6.1. Tensile testing. It is the measure of strength of a material that is measure of stress under which material undergoes plastic deformation or a stress against which material withstand. It is also the interest of its ductility. Special techniques are used for accurate measurement usually ultrasonic techniques are used to get more accurate measurements. Different factors that are involved in measurement of tensile strength are tensile machine and specimen stress strain graphs.

1.6.2. Test methodology and data analysis. Different methodologies are employed to test mechanical strength but the method that we employed is given below

1.6.2.1 Tensile machine and specimen. The specimen is usually enlarged from the ends. Or shoulders for gripping. The most important section of specimen is gage length. Gage section or gage length is area that is under testing over it measurements are made. Different types of machines are used for tensile testing. Most often electro mechanical machines contain a wide range of speeds and longer cross head displacements. On the other hand hydraulic machines are cost effective in case of high speeds [36].

Figure 1.18. Specimen for analysis

1.6.2.2. Stress-strain curves. When the sample mounted in machine it plots different curves, the force applied and elongation in specimen have very small values if it is not normalized.it could be normalized as stress and strain.

$$e = \Delta L/L0$$

Where e is strain, ΔL is change and L_0 is initial gage length. And nominal stress could be defined,

$$s = F/A_0$$

Where S is stress, A_0 is Initial cross-sectional area and F is applied force in Newtons.
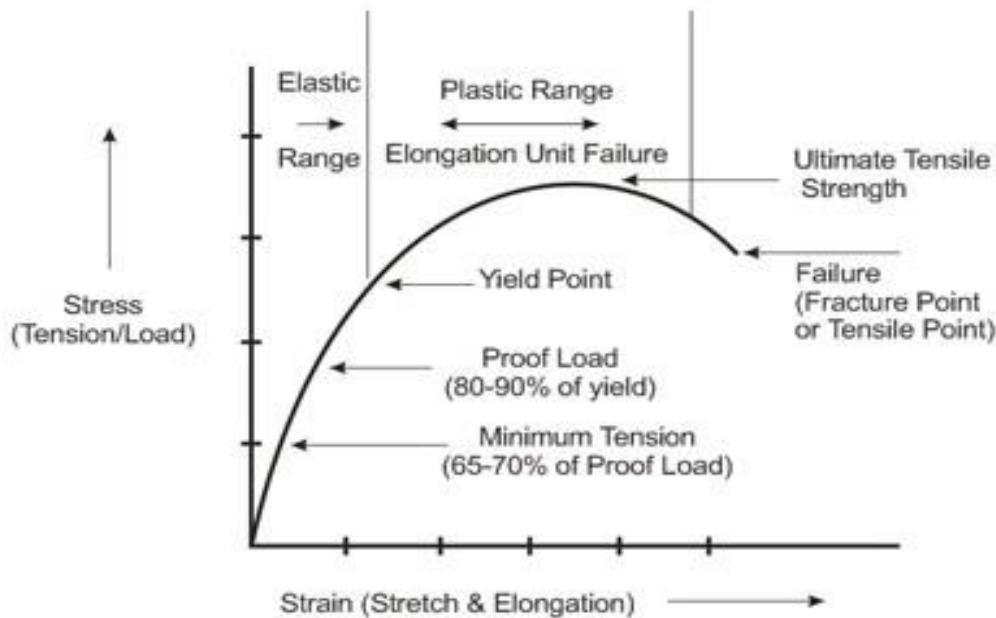
Figure 1.19.Analysis of different parameters through stress strain graph

The graph of tensile testing could be plotted between different parameters, but the stress-strain curve is most common as it is independent of specimen dimension. Stress application creates two types of deformations; Elastic and Plastic deformations. When the stress is applied on a material its bond stretched and relax when force removed is called as *elastic deformation*. If force increases the planes of atoms slide over each other and upon removing force it does not retains its shape is known as *plastic deformation*. Initially the stress-strain curve of most of the materials are linear, its slope is known as *elastic or Young's modulus.*

$$E = s/e$$

20

In stress-strain curve the ratio of lateral contraction strain to the axial strain is called as Poisson's equation, given below,

$$v = -e_y/e_x$$

After the plastic deformation starts the both elastic and plastic deformations play their role. Which is called as total strain it can be described mathematically as,

$$e_T = e_e + e_p$$

Proportional limit is the point at which linear stress-strain curve deviates. But to get appropriate reading 2% or 0.002 of the stress-strain curve is extrapolated to get the value of yield strength. It is the point at which line intersect the curve. Yield strength does not depends upon instrument [37]. There are many factors that affect the shape of stress strain curve including; Temperature, Strain rate and Anisotropy

1.6.3. Steps of tensile testing

a. Selection of material: The materials selected for the test should have all the characteristics of the bulk. One or more complete parts are sacrificed to obtain test samples from the most critical parts of the built-in sample.

b. Sample preparation: Sample should be prepared in such a way that all its axis must be aligned in materials rolling direction. Before testing it should be confirmed that gage length and testing area contains the materials characteristics and is according to the machines standard.

c. The test setup: There are three requirements of the machine; i). force capacity should be sufficient, ii) control of test speed (strain rate) and iii) precision and accuracy. For grips there are two rules for testing; i). the grips should fit the sample properly and ii). the grips should have sufficient force capacity.

d. Analysis of test data: Analysis of the data is done at several levels, at first, the researcher observes the processing of test either sample is slipping from jaws or the fracture occurs outside the gage section. After completion of test an equation according to the required data is applied and graph is plotted and required information is derived. For this database is used in which data may store for the future user. Rupture strain or micro strain could be calculated as

$$\epsilon_{rupture} = UTS/E$$

Where $\epsilon_{rupture}$ is rupture strain, UTS is ultimate tensile strength and E is modulus of elasticity.

21

SCHEMATIC DIAGRAM:
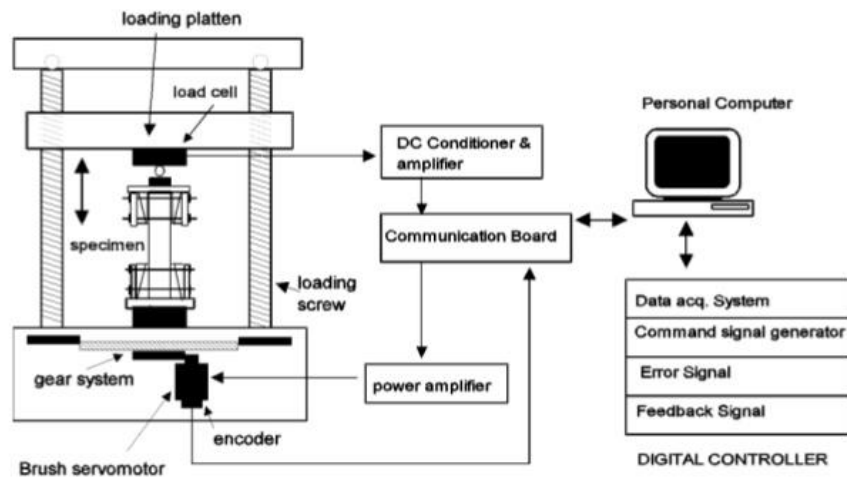
Figure 1.20. Instrumentation of tensile testing machine

Chapter 2

Literature review

2.1. Carbon nanotubes ceramics composite

This review is about different methods of synthesis for SWCNTs/ceramic and SWCNTs/ceramics/polymer composites. More specifically, the materials under consideration are nano transition metal oxides/CNT/polymer composites.

2.2. Methods used for composites preparation

Initially carbon nanotube composite with ceramics was prepared for the *in situ* synthesis of carbon nanotubes on a ceramic substrate due to many useful properties of carbon nanotubes and then extraction of carbon nanotubes was done. Like in 2000 E. Flahaut *et al,* used solid solution method to prepare CNT/Co/MgO composite by reducing MgCoO under H_2-CH_4 at 1000°C [38]. In same year E Flahaut, *et al,* extended the work to CNTs/(Fe, Co orFe/Co)/(Al_2O_3, MgO, Al_2O_4) composites, obtained by hot pressing. The electrical conductivities of all the composite lie within the ranges 0.2-0.4 S cm^{-1} [39]. In 2002 A. Peigney, *et al,* prepared CNT/Co/MgO composite by high temperature extrusion at 1050ºC to obtain dense product. The extruded rods were 6.7 mm in diameter and 20 nm in length. Electrical properties revealed that the by increasing the carbon content in composite, the conductivity increases. It was first time that carbon nanotubes were aligned in metal/ceramic matrix [40]. In 2003 Jing Sun and Lian Gao *et al,* proposed a method for CNTs dispersion in ceramics materials (Al_2O_3 and titania) by placing CNTs in a boat shaped tube at 600ºC in the flow of ultra-pure N_2 or NH_3. The four dispersant used were; a) poly acrylic acid (b) poly ethylamine (c) 4,5-dihydroxy-1,3-benzene disulphonic acid di sodium salt (d) sodium dodecyl sulphate [41]. In same year Guo Dong Zhan *et al,* investigated the spark plasma method to form alumina and single walled carbon nanotubes. Both alumina and SWCNTs were mixed separately into ethanol than both were mixed by using spark plasma sintering technique. They prepare two composites one of 5.7 vol %of SWCNTs and other was of 10 vol % of carbon nanotubes the high temperature was provided by electrical discharge and 623 MPa pressure applied at 600ºC. The refinement in grain size due to carbon nanotubes was observed. It was seen that with the

increase in density toughness also increases. It leads to the reinforcement of Nano ceramics [42]. Most of metal oxides and CNT composites used in super capacitors as CNT allow the improvement in electronic conductivity. Different dimensions of the composites could be prepared and could be used in different ways [43]. In 2004 S. Rul *et al,* prepare 22 different composites containing 0.23 and 24.5% vol of carbon nanotubes. The solution of oxide powder or ceramics was prepared by nitrate urea combustion method. And by attritor miller method ceramic foam was prepared. The organic content was removed by calcination. The *in-situ* synthesis of single walled carbon nanotubes was done under H_2-CH_4 gas mixture. The temperature was 1000ºC the mixture was hot pressed in a graphite die at 43 MPa.in secondary vacuums at 1300ºC. The dense pellets were obtained and polished by two faces. The carbon content was measured by flash combustion method. The densities of all the composites were also measured by their weight and dimensions fracture surface of the carbon nanotubes were also observed. By high resolution FEG-SEM and HRTEM, electrical conductivity was also measured by increasing dc voltage. It was observed that electrical conductivity increases as you increase the vol % of the carbon nanotubes.[44].

In same year X. Wang prepared the composite of ceramics and single walled carbon Nano tubes and graphite with ceramics. The high density Al_2O_3 was prepared and was dissolved in methanol and composite was prepared with graphite and single walled carbon nanotubes by spark plasma sintering the 10% vol. of single walled carbon Nano tubes. Single walled carbon nanotubes were characterized by Raman spectroscopy. The spark plasma sintering was done at 1550ºC in vacuum. Vickers indentation shows cracking. The toughness was determined by SEVNB. The Hertezian Indentation test was also done to check the toughness results. The techniques used for different characterization purposes were SEM to check the fracture of the surface and TEM. The Hertezian cracks were observed. The mechanical behavior was studied it was reported that homogenous and heterogeneous composites show different shear the heterogeneous composite shows weak shear [45].In 2008 Erica L. Coral *et al,* investigate the method of making composites through colloidal dispersion and the aqueous suspension composites were formed. The surface stabilizers or surfactants were used at low pH. The fabrication of single walled carbon nanotubes at 1%, 2%, 6% vol the technique of rapid prototyping was used. To determine the single walled carbon nanotubes Raman spectroscopy was used and to make composite spark plasma sintering was used at 1800ºC. The densities were 97% than the theoretically calculated densities. In the process the metal catalyst was used to purify single walled carbon nanotubes. The surfactant or cationic catalyst that was used as

stabilizer was cetyl trimethyl ammonium bromide (CTAB). Above critical micelles concentration the micelles were formed having bromide group at the head and in water the bromide ion dissociates to form positive charged head. The X-ray absorption or sedimentation technique was used to measure the particle size. The powder of composite was prepared by de ionized water. The different measurements and tests were conducted with or without single walled carbon nanotubes. It was followed by ultra-sonication. Electro acoustic analyzer was used to measure potential. Strained controlled rheometer was used to do viscosity measurements. Parallel plate fixture was used for different potential measurements. The gap size determine was 1 mm to 1.6 mm and sheer rate was 0.1-100 s^{-1}. Different suspension of silicon nitride in aqueous media was prepared and 2 suspensions per pH profile were used for measurement of mechanical properties. Spark plasma sintering was used at 5000A and voltage of 10 volts. micro hardness was tested by diamond tip.to test the tolerance of composites a series of increasing load was used, and grind ability was also tested.to investigate the effect of experimental variables the method of pre-cracked beam was employed. It was novel Si_3N_4 and carbon nanotubes composite that shows the increase in grind ability of the ceramic but increase in toughness was not observed [46]. In 2010 Chen Po Chiang et al first time uses transition metal oxide composite with single walled carbon Nano tubes for a symmetric super capacitors the ruthenium oxide (RuO_2) and indium oxide (In_2O_3) were used and the single walled carbon nanotubes and transition metal oxide composite was used as positive electrode and the electrolyte used was neutral the electrolyte was tetraethyl ammonium tetrafluroborate ($TEABF_4$) in acetonitrile.

The MnO_2 nanowires and In_2O_3 were coated on the carbon nanotubes that eliminates the water splitting the electrodes were optimized. The conditions were as follows: 2V, 184 F/g capacitance, energy density was 25.5 W/kg and power density were 50.3kW/kg. Single walled carbonv nanotubes were also used as current collecting electrode [47]. In 2011 XIAJUN Zhang *et al,* prepare CuO Nano belts using wet chemical method and then it was mixed with single walled carbon nanotubes and used as pseudo capacitor. And single walled carbon nanotubes were used to collect the current the conditions applied were current density of 5 Ag^{-1}. In potential range of 0-2.5 V the electrodes were obtained after 1000 cycles in 1 M LIPF/ECI: DEC [48].In 2012 Ali Can Zaman *et al,* prepared the alumina and single walled carbon nanotubes by a novel method the alumina having particle size 0.2 micrometer were taken and their suspension was prepared. Single walled carbon nanotubes having two different functional groups were dissolved in ethanol and ball milled for 3 hrs and was also ultra-sonicated for 30

mins. The same procedure was repeated with alumina and then both suspension mixed together by continuous magnetic stirring. Than the resulted composite was ball milled for 3 hrs. Than dried in oven at 100ºC. Spark plasma sintering was employed at 1600ºC under 50 MPa.

The holding time was 5 mins with the rate of heating 40C/s. the diameter of sintered pellets was 20 mm. The characterization techniques used were SEM, TEM and FEG. Grain size was 3.94 g/cm^3. Vickers micro hardness method was employed to check hardness. Electrical properties were studies and it was seen if carbon nanotubes arrange along grains the electrical conductivity increases even at low carbon nanotube content. The average grain size of composite for COOH-SWCNT/Al_2O_3 was 2.11µm and for OH-SWCNT/Al_2O_3 was 2.28µm [49]. In 2013 D. Silambarasan et al prepare single walled carbon nanotubes and SnO2 composite for hydrogen storage. The single walled carbon nanotubes of 99% purity were employed and the composite with SnO_2 was prepared having ratio1:2 weights. Then by using agate motor the composite was well ground for 15 mins. The uni axial pressure of 5 MPa was applied and the pallets of composites were obtained these pallets were then converted into glass films having dimension of 25 mm x 75 mm x 1.35 mm. these glass plates were cleaned with chromic acid or acetone. Sonication was done, and these were placed in water cooled graphite crucible and evaporated at glass substrate the hydrogen was allowed to flow from vacuum chamber and then hydrogenation was done on the glass substrate. Before it the hydrogen was thermally breakdown and converted into atomic hydrogen. The characterization techniques used were SEM, TEM, AFM, XRD, EDS, and TG/TDS. It was seen that much amount of hydrogen could be stored and can be desorbed easily by heating due to presence of carbon nanotubes [50].In same year D. Silambarasan *et al,* investigate that single walled carbon nanotubes and alumina composites could be used as substrate for hydrogen storage. The carbon nanotubes used were > 98% pure and the alumina was 99% pure. The carbon nanotubes were first purified by heating up to 300ºC for 1h. The carbon nanotubes were mixed with mixture of nitric acid and sulphuric acid. Then ultra-sonication was done for 8h and left behind over night the mixture was than filtered and dries and composite was prepared by taking 1:2 of single walled carbon nanotubes and metal oxide/alumina and ground well for 30 mins. Than mixture with propanol was sonicated for 3h to allow uniform dispersion. The dispersed solution was then deposited on alumina substrate the propanol evaporated and composite obtained than hydrogen was flowed through it and stored to check the adsorption of hydrogen desorption was done by annealing.

Thermal annealing was done at 300ºC for 1h. Raman spectroscopy was used to characterize the single walled carbon nanotubes and TEM was used. It was observed that average diameter

of carbon nanotubes enhanced to 20-25 nm due to attachment of metal oxide. The hydrogen storage capacity for CNT/SnO_2, $SWCNT/WO_3$ and $SWCNT/TiO_3$ was 1.1, 0.9 and 1.3 wt. % respectively. And desorption of hydrogen was very easy [51].Then in same year Biuck Habibi *et al,* used carbon single walled and ceramic composite as electrode. In experiment doubly ionized water was used. Three cell electrode systems were used and the copper wire was inserted into the ceramic electrode to establish the electric contact. The electric properties were measured by different techniques. Volta metric calculations of different pharmaceuticals were done. Highly mesoporous interlinked 3D structure was observed. Electrochemically accessible surface area was observed. Interface was investigated and applicability of electrode was investigated [52].In 2014 R. Lavanya functionalizes the single walled carbon nanotubes with TiO_2 first of all the metal oxide was attached at the outer surface of the carbon Nano tubes and threshold set was 1×10^{-5} eV in energy and 0.5×10^{-3} eV in force. The repulsion was minimum at 2.75 A. after this the structure was allowed to relax and the metal oxide goes into the inner layer. Total 8 molecules were attached without dimerization than the hydrogen molecules were attached with metal oxide molecule by H-H bond. And the bond length was 0.75 A. as the composite formed the conduction started immediately [53].In 2015 M.H Bocanegra-Barnal *et al,* prepare the composites of different three types of carbon Nano tubes the multiwall carbon nanotubes, double wall carbon nanotubes and single wall carbon nanotubes composite with alumina matrix was prepared the Al_2O_3 used was >99.9% pure and the grain size was 5-10 m^2g^{-1}. The method obtained was as follows first of all the carbon Nano tubes were dissolved in ethanol and was ultrasonicated for 4 h. than in that suspension alumina powder was added with intense stirring so that ethanol completely evaporated. The substrate thus obtained was dried at 100ºC. the powder obtained was ground in agitate mortar.

The fabrication was one by spark plasma sintering at 1500ºC at heating rate of 100ºC min^{-1}. Maximum pressure was 80MPa.density was measured by Quadra chrome multi pycnometer. He was used as displacement gas. The characterization techniques used were FEG SEM, SEM, TEM, and HRTEM [54].In 2015 Yao Yuan et al makes the composite of single wall and multiwall carbon nanotubes with TiO2. The three types of anatase were employed. The small grain size anatase, the large size anatase, and mixed phase anatase. The carbon nanotubes were functionalized by mixing with nitric acid. Than the composites were prepared by simple evaporation and drying methods and their characteristics were studied [55].In 2016 Sangram Muzdar employed InSitu synthesis of carbon Nano tube ceramic with alumina the iron (II) chloride was used as catalyst for synthesis of carbon nanotubes the ceramic was prepared

directly foaming technique. The alumina mixed with silicon dioxide and the foaming was done by hand mixer. Propyle gallate was used as modifying agent. Ultra-sonication was done and the sintering technique was employed at 1300ºC for 1 h. NaZ was prepared and immersed with ceramic material and then subjected to $CoCl_2$ for ion exchange and CoZ was coated on ceramic and then catalytic decomposition of ethylene was done for preparation of carbon nanotubes in horizontal tube furnace [55].

2.3. PVA

As PVA is commonly known polymer and is used in various applications. A research was done to observe mechanical properties of PVA using AFM technique by force indentation and area-depth curves. The research indicate that two different methods to obtain young's modulus gives identical results [56]. By adding PVA in different types of concrete mixture large value of young's modulus was observed [57]. PVA hydrogels could be used as protein career. PVA and its blends with different types of materials are used for biodegradable packaging [58] [59].

2.4. PVA/CNT Composites

Previously CNT/polymer film was prepared by melt blending method the mechanical properties of PVA/CNT and PMMA/CNT were investigated and it was observed that CNT's well dispersed into the polymer matrix and enhance the tensile strength of the polymer [60]. The mechanical, electrical and thermal properties of CNT's in polymer matrix were investigated. It was observed that with addition of carbon nanotubes in polymer matrix these properties enhance significantly [61]. SWCNT in PVA matrix were fabricated by electrospinning method and enhancement in mechanical properties were observed through stress-strain curve [62].

2.5. PVA/MO composites

Composite of PVA with TiO_2 was analyzed and it was used for filtration applications the membranes were prepared by electro spinning method. The mechanical behavior of the composites with different concentrations of TiO_2 was observed and it was evaluated that by increase in concentration of TiO_2 strain rate decreases and tensile strength increases. Good photocatalytic activity of the composites was observed [63].

2.6. CuO/CNT composite

The glassy carbon electrode was modified by CuO/CNT by doping method and electro activity towards hydrazine was observed. Cyclic voltammetry and ampere metric experiments were carried out to check electro activity [64]. in 2014 CuO/CNT composites were used as antimicrobial high performance material the enhancement in mechanical properties was

observed [65]. Recently in 2016 Revendra kumar singh et al used precipitation method to prepare CuO/CNT composite and used these composite as Nano adsorbent for adsorption of As$_{(III)}$ and As$_{(v)}$ water and the uptake capacity calculated was 2267µg^{-1} for As$_{(III)}$ and 2395 µg^{-1} for As$_{(v)}$ [66]. CuO-CNT 3D network w3as prepared in 2013 by using electrostatic interaction in aqueous solution. Electrochemical performance was evaluated, and it was improved greatly. The modified electrode was 2.3 times more efficient as compare to pure CuO Nano sheets [67].Later on CNT coated film was prepared and coated on Cu nanowires to enhance the field electron emission. The turn on field of CuO was observed to be decreased to 1.2 V/µm from 6.6 V/µm. drop coating was use and hydrothermal method was used to grow CuO Nano wires. In that experiment two types of materials were prepared CuO needle like structure and Nano wires were wrapped in CNT's and CNT on the surface of nanowires shows effect on the turn on field and emission stabilities [68]. Mesoporous CuO that were prepared in another experiment were oval in shape and were threaded in MWCNT that were used as conductive path high interface was created and due to porosity of CuO it allows the Li ions to pass through them. CNT shows enhanced electronic conductivity it also allows the long term stability of the anode. The anode prepared showed remarkable electrochemical performances. High rate capability, stable capacity retention and reversibility was observed [69]. Recently the CuO oxide/Reduced graphene oxide and carbon nanotube composite was prepared for biological and clinical purposes as biosensor to detect glucose level in order to treat diabetic patients. It was used as alternative for enzymatic biosensor that were specific and with little life time [70].

CuO and its composite with carbon fibers or CNT grabbed attention towards their uses in lithium ion batteries as CuO shows inelastic pretties and could be used as an alternate of graphene electrode due to its reversibility and high capability [71]. Another researcher examined the CuO-PAA/CNT film for super capacitor. Composite was annealed at different temperatures and annealing effect on supercapacitor was studied. Different techniques were employed for characterization and it was observed that C$_{SP}$ increases from 188 to 258 Fg^{-1} as annealing temperature increases [28].By some other researcher the composite of Cu doped Ni was prepared with CNT and CV,EIS and galvanic charge discharge test was performed. As CuO also act as catalyst it shows high columbic activity and better retention capacity [72]. The use of CuO nanobelts with carbon nanotubes was reported for their use in pseudo capacitors electrodes as they show good cycling ability as the electrode of composite is more flexible and shows higher specific capacitance as compare to pure CNT electrode. Specific capacitance of hybrid film was > 62 Fg^{-1} after 1000 cycles and for pure SWCNT it was only 23.6 Fg^{-1} [48]. For

lithium ion batteries the composite of CuO in 3D structure of CNT were prepared by simple solution method and improved cycling capacity and buffering capacity was measured [73].

2.7. NiO/CNT composites

Porous NiO and CNT were used as electrode for pseudo supercapacitor were used and KOH was used as an electrolyte. They show high storage capacities. Different concentrations of CNT were used and their specific capacitance was measured 10%, 30% and 50% CNT shows 2709,242 and 112 F/g at the charge of 0.56 A/g and maximum specific capacitance was 329 F/g at charge of 0.33 A/g [74]. Highly sensitive sensor of NiO and CNT was prepared to determine the BPA in food samples. A decrease in overpotential of BPA with 2.3 folds increment was observed. Results shows that oxidation peak current was proportional to the BPA [75]. The use of CNT and NiO oxide for yarn supercapacitors in the field of flexible electronics was investigated in a research. simple electrodeposition method was used to deposit transition metal oxide on the CNT and their mechanical behavior was observed [76]. Successive ionic layer adsorption was used to deposit layer of NiO/CNT directly on the steel substrate. Impact ratio of adsorption and electrochemical properties were investigated.

High specific capacitance 1727 F/g at 5 mA/cm^2 of current density 91%capacitance retention after 2000 cycles [77]. By using vacuum annealing and oxygen plasma treatment NiO were grown directly at CNT on carbon substrate. Low internal resistance observed. The electrode capacitance that could be achieved was 162.41 F/g while simple CNT electrode shows 53.75 F/g. from these results it was concluded that NiO based CNT composites were suitable for EDLC applications [78]. Most of the NiO and CNT composites were investigated in order to enhancement of storage devices in field of EDLC in some aqueous capacitors. These composites provide both the desired power and energy densities [79]. Previously NiO/CNT composites were prepared by simple precipitation method. By the addition of CNT network into host NiO the conductivity improved and it enhance the surface area of the material. It also improves the power density and cycle life. The 10% of CNT shows stability over 100 cycles.it could be used as alternative for activated carbon that have low cycle, life. It was observed that when annealing temperature increases the capacitance increases respectively. In turn it may decrease surface area and it result in less active sites [80].

For microbial fuel cells instead of precious metals non precious transition metal was selected to reduce the cost and oxygen reduction reaction efficiency. The cyclic voltammetry and rotating ring desk electrode test was performed and it was observed that oxygen reduction peaks were observed. The power observed was 670 mW/m^2 and 0.722V of OCV were obtained

[81]. Electrophoretic deposition was used to grow the film of CNT supported with NiO. Hydrothermal synthesis was used and high specific capacitance of 1151 F/g was observed at high discharge current of 50 A/g [82]. Another researcher investigated another aspect of the NiO/CNT composite in ionic liquid to detect Nalbuphine an analgesic drug electrochemical investigation was carried out. And catalytic effect on oxidation of nalbuphine was observed. Linear dynamic range was 500 µmol/L NA with detection limit of 0.07 µmol/L NA [83]. A few years before a research was done on use of NiO/CNT composites for supercapacitor electrode.

$$C = Q \backslash V$$

Due to large surface area high conductivity and long life cycles these composites gain the interest of many researchers [43].for Hydrogen evolution hetero-structure of nanoscale nickel oxide were grown on the wall of single walled carbon nanotubes as highly effective electro catalyst. The hydrothermal decomposition of nickel hydroxide was carried out that was banded with the sidewalls of carbon nanotubes [84]. Recently a research is reported in which nonporous nickel oxide material was used as catalyst for oxidation of carbonates and carboxylates that were incorporated on the carbon nanotubes and this was used as electrode for lithium-oxygen batteries [85]. Different metal oxides catalysts were loaded on the single walled carbon nanotubes and OER result of 50% NiO/CNT catalyst was most active with an onset potential of 1.45 V versus RHE [86]. NiO/CNT composites were prepared by simple hydrothermal method and their electrochemical properties were measured in dodecyl sulfate system it was observed that by changing dodecyl sulfate concentration the morphology was changed and zero dimensional mesoporous NiO on CNT surface shows the good specific capacitance 1329 F/g and very good cycle life as 1000 cycles in 1molar KOH solution at high current density 84 A/g [87]. A research was reported on super-aligned carbon nanotubes and metal oxides were grown directly on them for their use in super capacitors one step *insitu* decomposition strategy was used and very good specific capacitance was observed ~500 F/g reliable electrochemical stability < 4.5% degradation in 2500 cycles and very high rate capability 245 F/g at 155 A/g [88]. Syed Mustansar Abbas *et al*, in 2013 investigated the fabrication of NiO on CNT via polyvinylpyrrolidone through co precipitation method at current density of 100 mA/g initial reversible capacity was 962 mA h/g and after 50 cycles it was 601 mA h/g [89]. Electrolytic catalytic activity was analysed for NiO and CNT composites. The composite was prepared by deposition sodium hydroxide onto the carbon nanotubes and then annealing it.

2.8. Motivations and Objectives

Motivations. Through literature it was seen that a lot of materials were reported carrying good charge storing ability but the problems that were not sorted are.

- Low elasticity of MO
- Control of Transparency of materials carrying *f*-SWCNT/Polymer/MO
- Development of method to *f*-SWCNT withot damaging.

Objectives: There was need of a method to prepare a material that have

- High capacitance value
- Appropriate band gap
- Good transparency
- High mechanical strength.

Goal of the study was to achieve above mentioned goals.

Chapter 3

Experimental

It is a multistep procedure to prepare the CNT/PVA/M-O thin film composites. The chemicals used in the experiment were; H_2SO_4 (97% pure), HNO_3 (67% pure), $NiNO_3$ and $Cu(NO_3)_2.3H_2O$ both were of analytical grade purchased from RDH while PVA was of commercial grade with molecular wt. 86.09 g/mol. Single Walled Carbon Nanotubes (SWCNTs) purchased from He, Ji Inc.

3.1. Synthesis

3.1.1. Metal oxides. Metal Oxides were synthesized by previously reported methods NiO nanoparticles was prepared sonochemicaly [90] and CuO by precipitation method [91].

3.1.2. CNT's Purification. It is necessary to purify the CNTs before further use in order to get rid of different carbonouse and metal (catalyst) impurities by method reported elsewhere [92],[93]. Surface functionalization of CNTs was also ensured in order to get strong and durable composites with PVA and nanoceramics the metal oxides (MO).
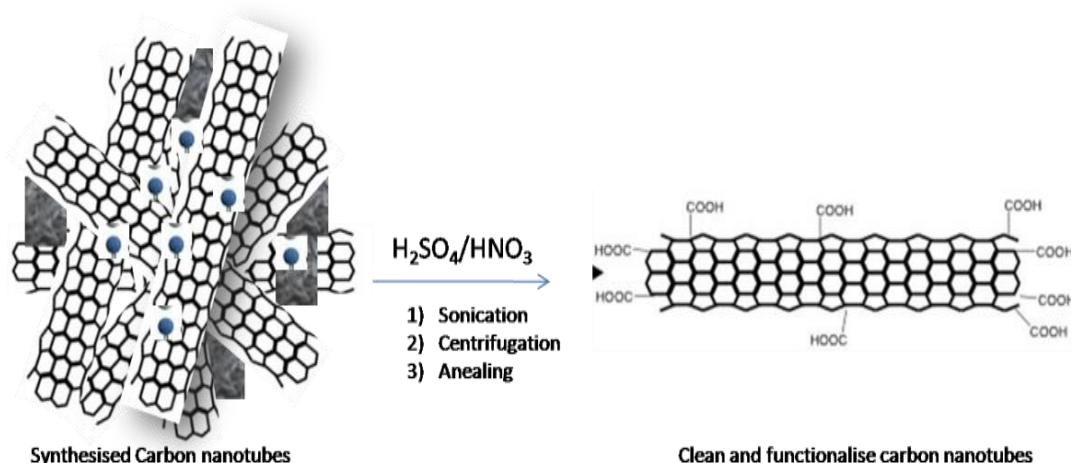
Figure 3.1. Functionalization of SWCNT's

3.1.3. Composite preparation. The purified and functionalized CNTs were sonicated for 3 h after mixing with different metal oxide (MO) nanoparticles ratios in distilled water in order to ensure homogenous dispersion. This CNT/MO mixture was added to the PVA solution under

constant stirring. The concentrations of CNTs and PVA were optimized, while different composites were prepared by varying the MO nanoparticle contents, Table 1 enlists various compositions.

Table 3.1. Concentration of different samples prepared

Sr.no	Sample Code	Concentration of reagents used (grams)		
		SWCNT	NiO	CuO
1	CN 1	0.01	-	-
2	CN 2	0.02	-	-
3	CN 3	0.03	-	-
4	CP 1	-	-	0.01
5	CP 2	-	-	0.02
6	CP 3	-	-	0.03
7	NP 1	-	0.01	-
8	NP 2	-	0.02	-
9	NP 3	-	0.03	-
10	CCP 1	0.01	-	0.01
11	CCP 2	0.01	-	0.02
12	CCP 3	0.01	-	0.03
13	CNP 1	0.01	0.01	-
14	CNP 2	0.01	0.02	-
15	CNP 3	0.01	0.03	-

3.1.4. Thin Film Preparation. Above prepared solution mixture was stirred for 7 h to achieve homogenous suspension. Thick solution was transferred to the glass substrate for water evaporation under vacuum drying for 17 h at 55ºC. Using the same route, thin film of PVA/CNT and PVA/MO were prepared, figure 19 depicts a flow sheet for this description.
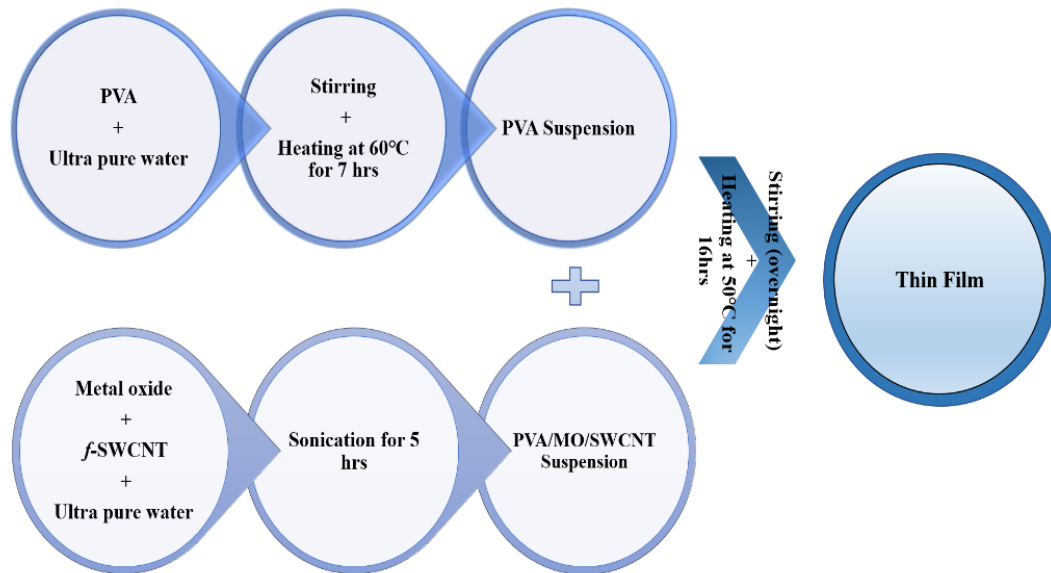
Figure 3.2. Schematic illustration of thin film preparation

3.2.   Characterization

X-Ray Powder Diffraction (XRPD) was done by employing STOE Germany X-Ray diffractometer operating at 40 kV with Cu Kα radiation within $10° \leq 2\theta \geq 80°$ range for powder and film samples. Field Emission Scanning Electron Microscopy (FESEM) analysis was done on MIRA3 TESCAN Zeiss supra 55VP for qualitative and morphological testing of powder and film sample after Au coating. AFM was employed to observe Topography of samples and 3-D images were captured by using high resolution, high performance environmental scanning probe microscope (JSPM-5200) WINSPM version 5 using tapping mode. Fourier transform Infrared Spectroscopy (FTIR) was performed by using platinum ATR Model Alpha with spectral range 4000-550 cm^{-1} by placing the samples directly on diamond scanner.

3.2.1 Physical Properties. UV-Vis (single beam) spectrophotometer model T60 PG instruments UK, was also employed to check the transmittance and to confirm the band gaps through absorbance co-efficient. Perkin Elmer UV Vis DR Spectrometer Lambda 950 with spectral range was 190-3300 cm^{-1} was employed for optical properties and band gap calculations. For dielectric properties measurements thin films were cut into the 2 mm diameter circles and pressed between electrodes of LCR meter model; Wayne Kerr model 6500 B with

frequency range 100 Hz to 5MHz. Tensile testing was done using standard ASTM D638-12 of UTM (AG-X Plus) Shimadzu Japan for the samples with gage length; 20 mm and width; 1 mm under 10 N applied force at the speed of 5 mm/min.

Chapter 4

Results and Discussion

This chapter deals with the result details and discussion over these findings.

4.1. Characterization

4.1.1. FTIR. First of all cleaned and functionalized CNTs were analyzed via FTIR spectroscopy in order to ensure the functionalization of SWCNT. The spectrum depicted in figure 4.1 shows (after base line correction all bands become obvious) the bands of sulphates (SO_X) near 602 cm^{-1}. While different nitrates (NO_x) showed appearance as bands between 1738-2136 cm^{-1}. An intense band of C-H stretch was observed near 2136 cm^{-1} [94, 95] [12]. A broad -OH stretch was seen from 3213 cm^{-1} that of C=O at 1788 cm^{-1} [96].
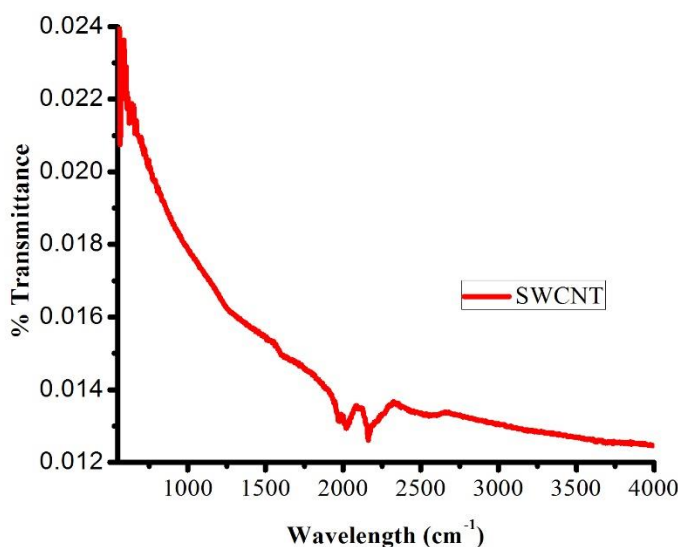
Figure 4.1. IR spectrum of f-SWCNT's

Figure 4.2 representing spectra of (a) PVA/MO and (b) PVA/MO/*f*-SWCNT.As CuO and NiO did not absorb between 400-4500 cm^{-1} it show absorbance or transmittance below 400 cm^{-1} so there was no band observed for CuO. And NiO [97] moreover the major bands associated with PVA were observed, a broad band of acetate C-O and C=O was seen between 1500-200 cm^{-1} large -OH band was also observed between 3300-3500 cm^{-1} [98]. In spectra Of composites CCP and CNP it was seen that the bands were present indicating presence of PVA that were

37

discussed above as well as incorporation of *f*-SWCNT was also confirmed as the bands indicating presence of CNT were seen however due presence of same bands of NiO and *f*-SWCNT the presence of both materials was confirmed by XPRD analysis [99],[100],[65].
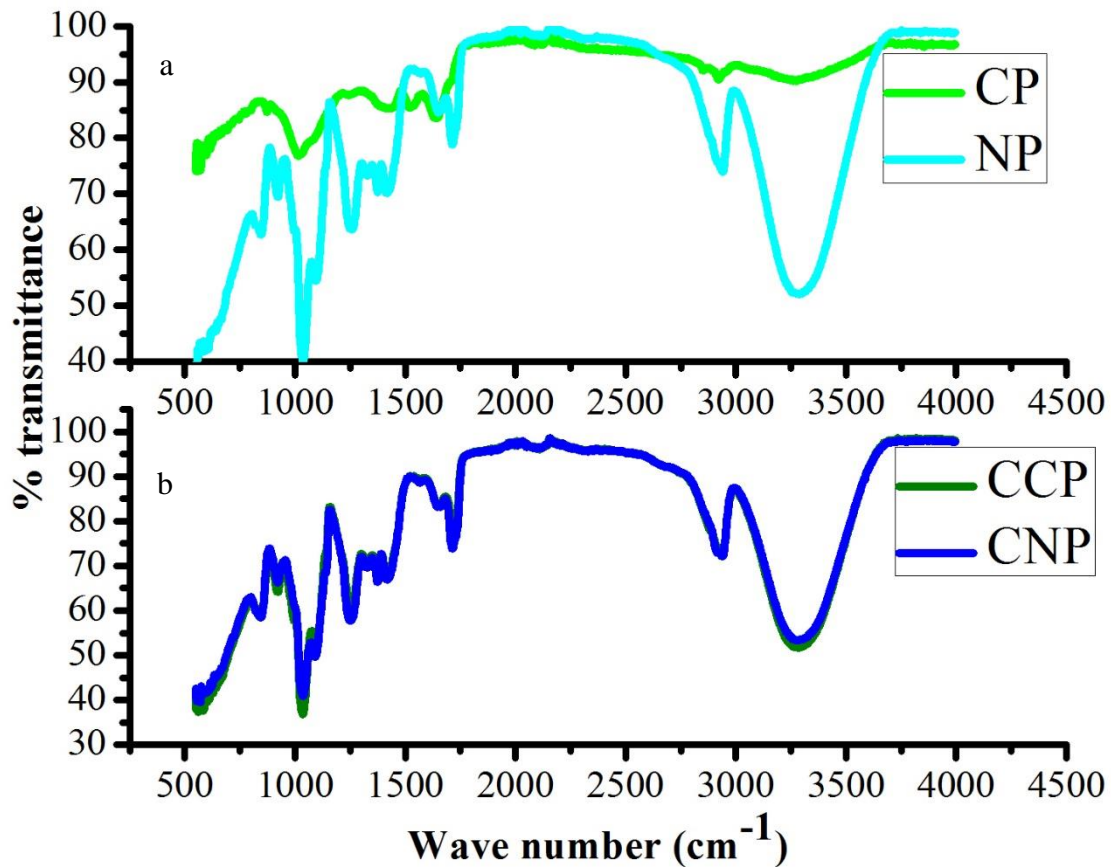
Figure 4.2. IR spectra of (a) MO/PVA (b) CNTs/MO/PVA composites

4.1.2. XRPD. XRPD data of pure nanoceramics was recorded and crystal structures were confirmed by comparing with literature, all peaks were indexed with JCPDS card no. 45-0937 and 73-1523 for NiO and CuO, respectively as shown in figure 4.3. The average crystallite sizes were calculated as 34.21 and 4.983 nm for NiO and CuO, respectively, by using Scherrer formula given below

$$d = K\lambda / \beta \cos \theta$$

Where, d is the crystallite size, K is the shape factor (0.9), λ is incident radiation wavelength, i.e. 1.54Å , θ is Bragg diffraction angle (º) and β is FWHM of the respective diffraction peak (in radians).
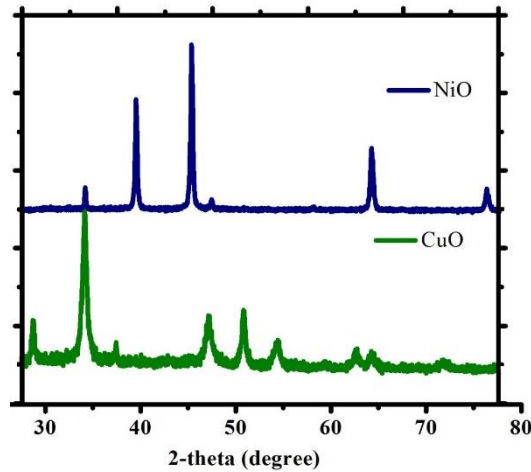
Figure 4.3. XRD spectra of NiO and CuO

XRD patteren of SWCNT before and after functionalizaion was recorded to clearify that if after functionalization structure of SWCNT's changes or not. By analysing Fig 4.4. It was observed that in case *f*-SWCNT two humps were obseved indicating the lack of crystalanity and compared with litrature[101] to confirm the functionalization of CNT. Absence of MWCNT peaks observed. When *f*-SWCNT incoporated into polymer matrix sharp peaks due to crystalline nature of PVA were observed that is the indication of ordered hexagonal structure of CNT and peak at 44° also indicates uniform dispersion of CNT in PVA [102] [103].
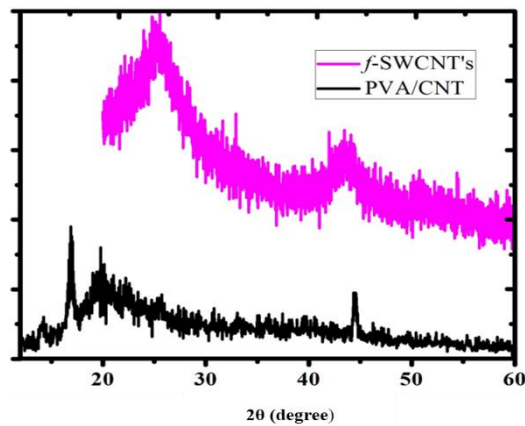
Figure 4.4. XRD partern of f-SWCNT's and PVA/SWCNT's

The Fig 4.5 shows comparison of NiO with NiO/CNT/PVA and CuO with CuO/CNT/PVA. It was seen that all the peaks of NiO, CNT and PVA were present in spectra but a little chemical shift was observed due to tilted film during analysis and also due to lattice strain that was produced in lattice during composite formation.
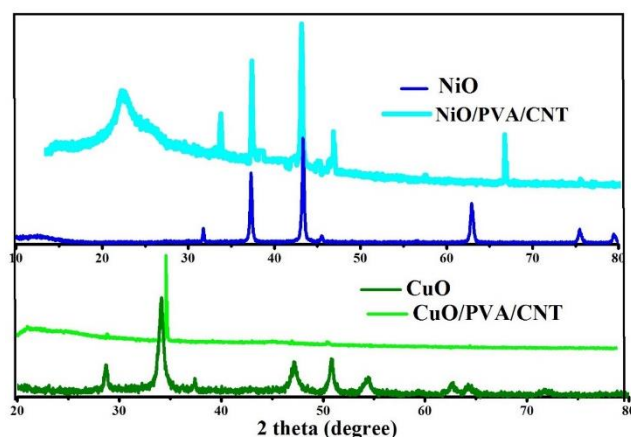
Figure 4.5. Comparison of XRD patterns of NiO, NiO/PVA/CNT's and CuO/PVA/CNT's

4.1.3. SEM. Fig 4.6 shows SEM micrographs of NiO/CNT/PVA and CuO/CNT/PVA analyzed at different resolutions a, b and c are showing micrograph of NiO/CNT/PVA at magnification of X10,000 in (a) and X20,000 in (b) at specimen distance of 1µm at voltage of 20 kV and 10 kV for a and b, respectively. It was necessary to analyze at lower voltage in order to avoid the film rupturing. In figure 4.6.c with specimen distance of 10 µm clear image of zigzag CNT was observed. Figures 4.6.d, e and f are showing composite CuO/PVA/CNT with homogeneous dispersion of *f*-SWCNT. In figure 4.6. e diameter was calculated that ranges from 44-88 nm for zigzag SWCNT dispersed in PVA.
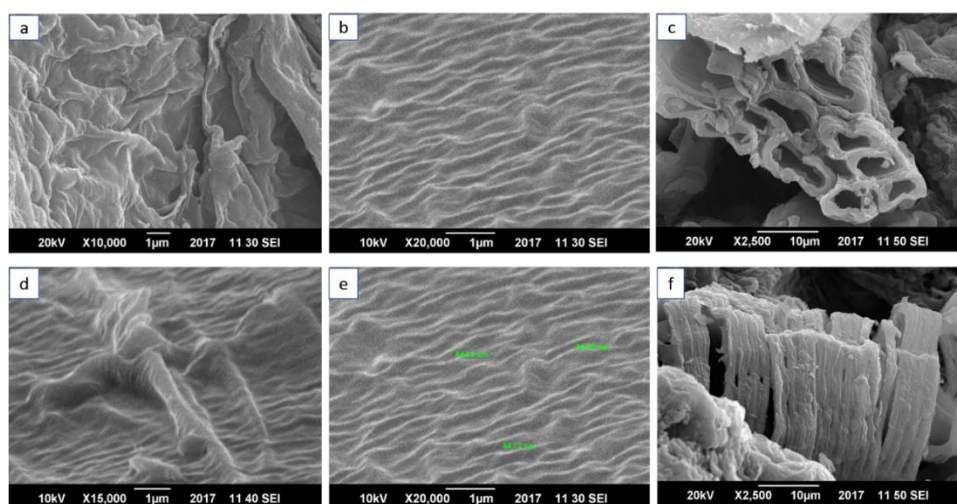
Figure 4.6. SEM images of (a), (b), (c) NIO/CNT/PVA and S(d), (e), (f) CuO/CNT/PVA

4.1.4. AFM. Atomic force microscopy was preformed to get 3-dimensional image of composites. Figure 4.7 shows 3-D images of (a) NiO/PVA/CNT and CuO/PVA/CNT. Analysis was performed under taping mode. 3-D images shows topography of the *f-SWCNT*.

40
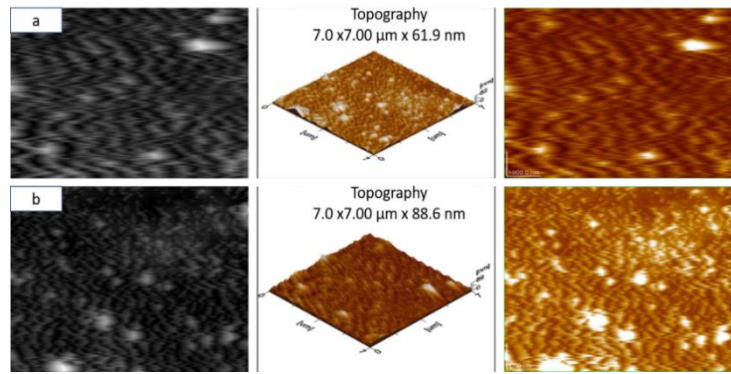
Figure 4.7. AFM images of (a) NiO/PVA/CNT's (b) CuO/PVA/CNT's

4.2. Physical Properties

In physical properties optical, dielectric and mechanical were measured. Optical properties were investigated in order to optimize the transmittance and to calculate band gap through UV-Vis. Whereas, UV-DRS was employed in order to confirm the band gap with reflectance measurements and dielectric properties to calculate dielectric constant, dielectric loss, tan loss and ac conductivity through LCR meter.

4.2.1. Optical Properties. With the help of UV-Vis spectroscopy, transmission as well as absorbance measurements were recorded. It was observed that minimum CNT concentration shows highest transmittance as shown in Fig 4.8, same trend was observed in case of MO. As concentration of metal oxide increases transmittance tends to decreases to maintain the batter transparency, amount of CNT was optimized so the least concentration of was selected to incorporate into composites. Figure 4.8 shows that in case of *f*-SWCNT maximum transmittance was observed at different wavelengths which is due to presence of different functional groups

41
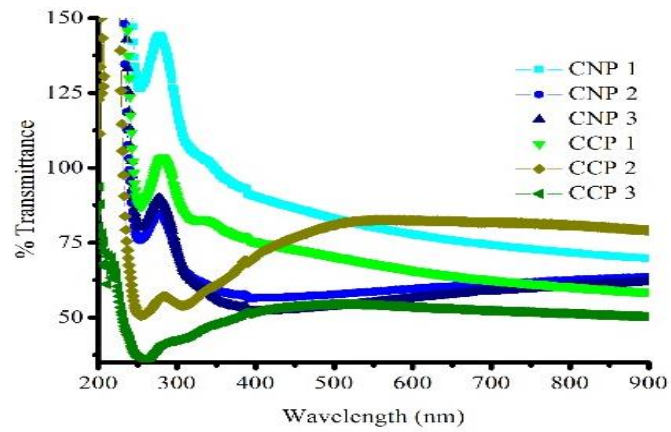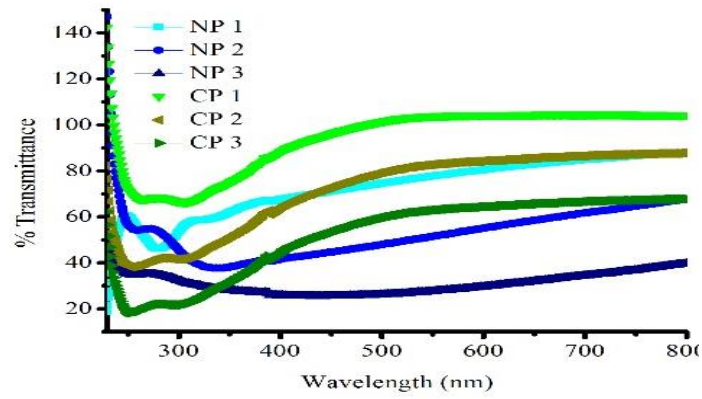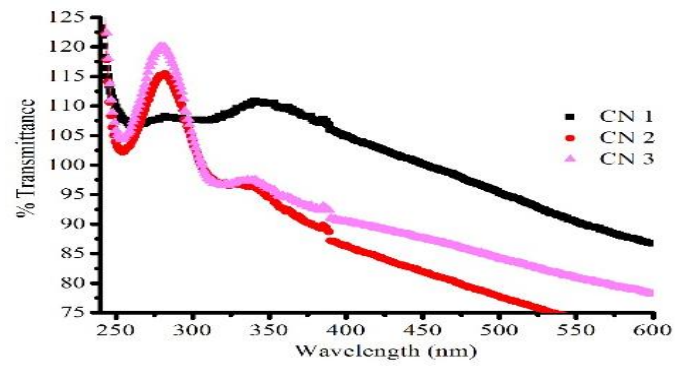
Figure 4.8. UV transmittance spectra of (a) SWCNT's (b) MO/PVA (c) MO/PVA/CNT's
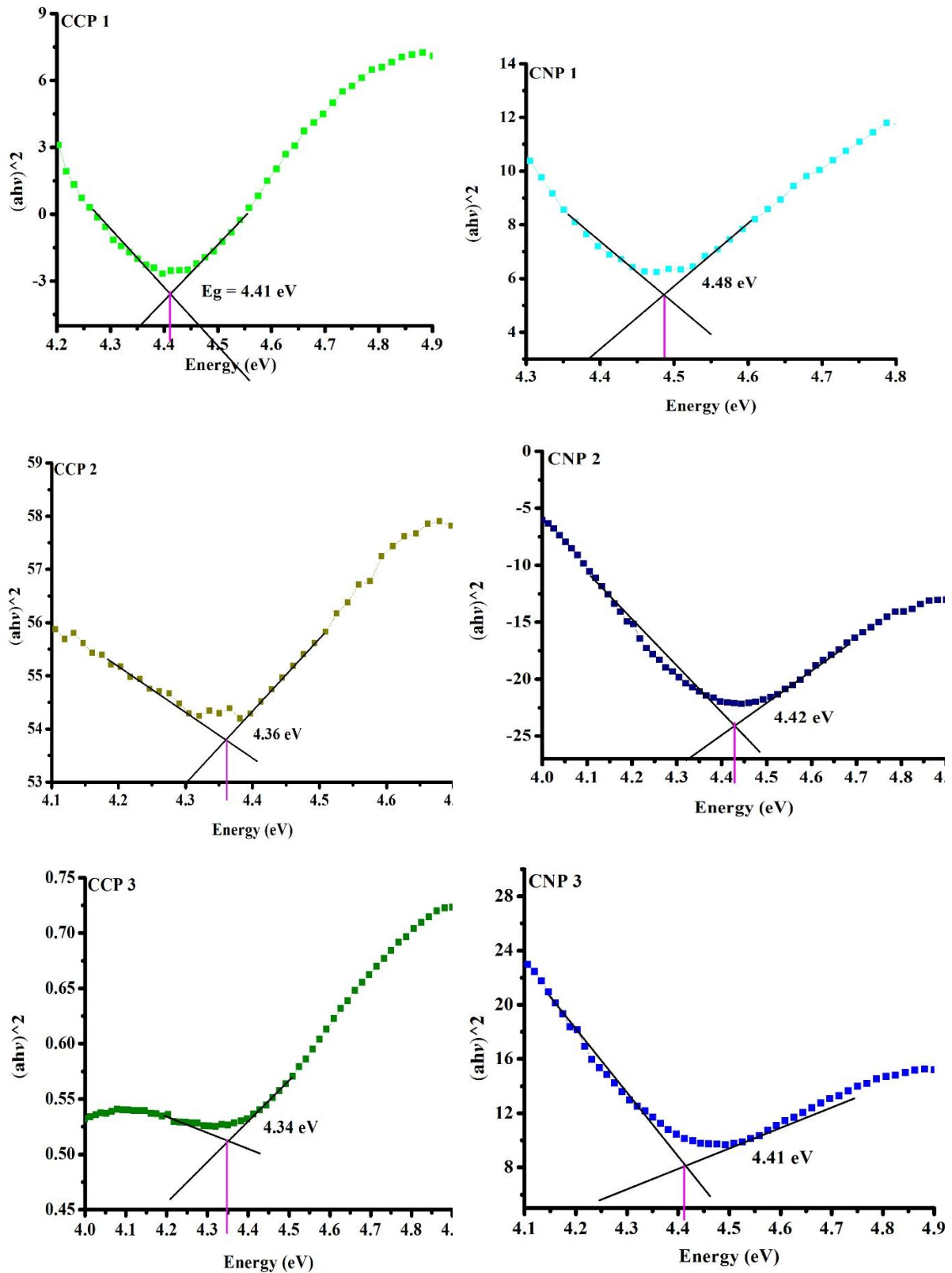
Figure 4.9. Band gap calculation through absorbance coefficient

Optical band gap calculations were done by UV-Vis in diffuse reflectance mode ranges from 200-1000 nm. Fig 4.10 shows graph plotted between reflectance (%) and wavelength (nm) it

was observed that all the compounds show the reflectance near ultraviolet region around 300 nm that was obvious. Band gap (E_g) was calculated by using Kubelka-Munk equation [104],

$$F(R) = \frac{(1-R)^2}{2R}$$

Where F(R) is reflectance coefficient (equivalent to absorption coefficient) and R is Reflectance. The graph was plotted between $(F(R) \times h\upsilon)^2$ and Energy (eV) as shown in Fig 4.11 to calculate the band gap [105] [106]. It was seen that by increasing NiO and CuO band gap decreases whereas the band gap reported for PVA in previous studies lies near 5-6 eV [107]. It was observed that by increasing amount of NiO and CuO band gap decreases as metal oxide particles arrange themselves in polymer matrix [108]. List of all the band gaps of sample is given in table 4.2.
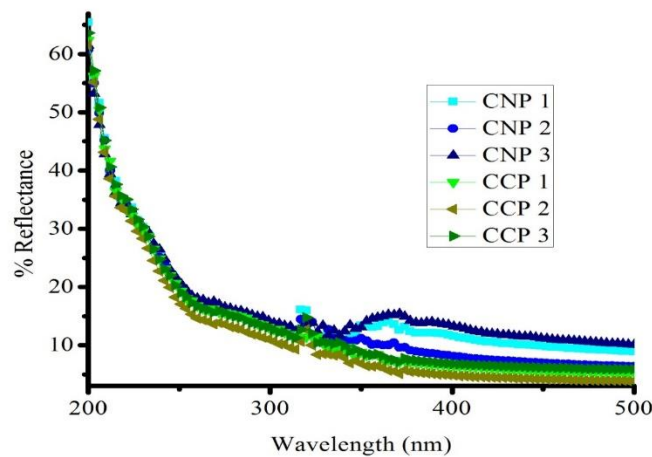
Figure 4.10. UV-DRS reflectance spectra of composites prepared
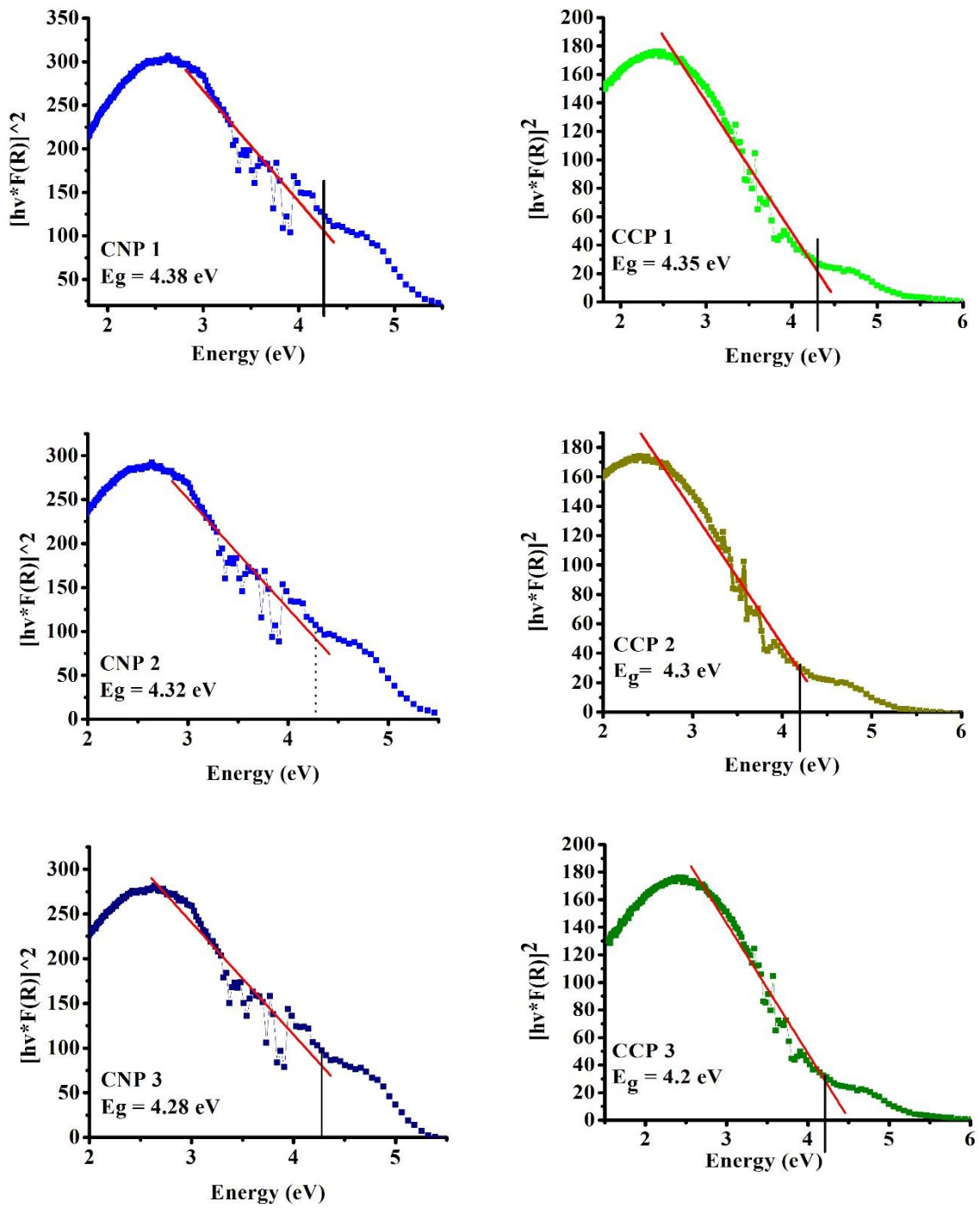
Figure 4.11. Band gap calculations of all the composites through reflectance coefficient

Table 4.1. Band gaps of all the samples prepared

Sr.NO	Sample	Band gap (eV) UV-DRS	Band gap (eV) UV-Vis
1	CN 1	4.40	4.42
2	CN 2	4.32	4.34
3	CN 3	4.10	4.22
4	CP 1	4.80	4.84
5	CP 2	4.70	4.72
6	CP 3	4.51	4.53
7	NP 1	4.98	4.92
8	NP 2	4.82	4.84
9	NP 3	4.61	4.65
10	CCP 1	4.35	4.41
11	CCP 2	4.30	4.36
12	CCP 3	4.20	4.34
13	CNP 1	4.38	4.48
14	CNP 2	4.32	4.42
15	CNP 3	3.28	4.41

4.2.3. Dielectric Properties. To study the application of prepared composites as capacitors, dielectric properties were carried out using LCR meter and processing the obtained data by using different equations discussed in upcoming sections. Different parameters investigated are dielectric constant, dielectric loss, tangent loss, and AC conductivity.

Dielectric parameter could be represented as [109].

$$\varepsilon^* = \varepsilon' - i\varepsilon''$$

Where, ε' is the real part, $i\varepsilon''$ is the imaginary part. The real part could be calculated as,

$$\varepsilon' = \frac{C \, X \, d}{A \, X \, \varepsilon_o}$$
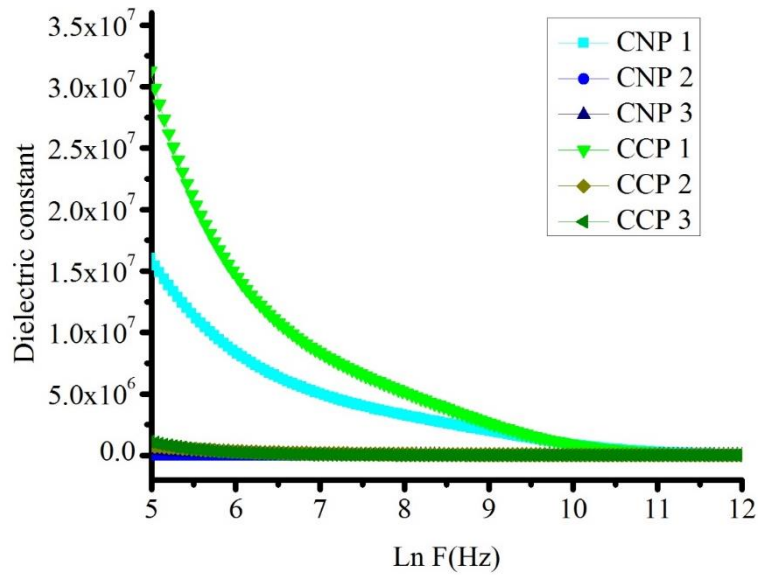
Figure 4.12. Dielectric constant measurements of all composites

This part explain the ability to transfer the charges or ability to store the charges of material.

Where, C is capacitance, d refers to thicknes (nm), A referst to surface area (m²), ε_o is the permitivity of space ($8.854 \times 10 - 12$ F/m). It was observed that as the frequency increases dielectric constant of the material decreases CNP1 and CCP 1 shows higher dielectric constants values that are 1.5 x 10^7 and 3 x 10^7, respectively, and dielectric it decreases with increasing amount of NiO and CuO as shown in Fiqure 4.12. It was seen that dielectric constant shows the frequency dependent behaviour as frequency increases. Dielectric constant is actually dependent on grain boundries that are created with in the material when external electrical charge is applied and high polarization achieved at low frequency as the frequency increases the priviously formed dipole fail to arrange themselves with fluctuating current so dielectric constant decreases and after certain value it become constant. It was seen by Fig 4.12. That as we increase the amount of metal oxides in material dielectric constant decreases it is due to poor separating boundries formation and also due to the porosity and defects. Dielectric loss is imaginary part that shows the heat dessipation and methematically can be calculated as,

$$\varepsilon'' = \varepsilon' \times Dissipation\ factor$$

Fig 4.13. shows the dielectric loss of values of all the composites prepared. Same behaviour was observed in case of dielectric loss as concenteration of MO increases dielectric loss value decreases as more energy will required for transfer of electrons from one atom to another atom and more heat dissipation will cause. As frequency increases atom did not show rapid electron transfer due to which dielectric loss value also decreases. As the frequency increases less

47

energy consumed for hopping of electrons and heat loss also become less at higher frequency [110]. CCP1 and CNP 1 shows highest dielectric loss values 1 x 10^8 and 3 x 10^7, respectively.
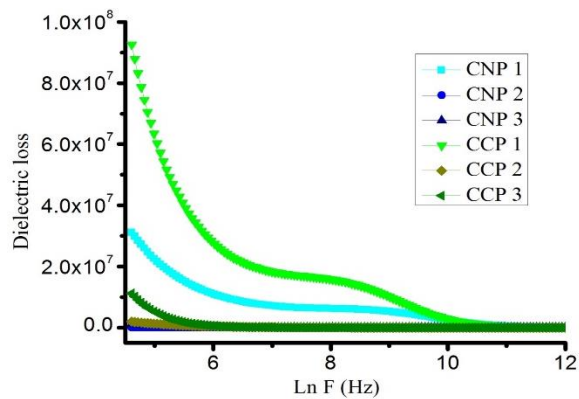
Figure 4.13. Dielectric loss measurements of all composites

Figure 4.13 shows the dielectric loss measurements of all composites that is actually the heat loss expressed in terms of tan loss, mathematically it can be expressed by following formula

$$tan\delta \ = \ \frac{\varepsilon''}{\varepsilon'}$$

Tan loss (tan δ) is relative measure of energy loss. Resonance peaks of CNP1 and CCP 1 were observed with increasing amplitude at low frequency it is actually the point at which frequency of
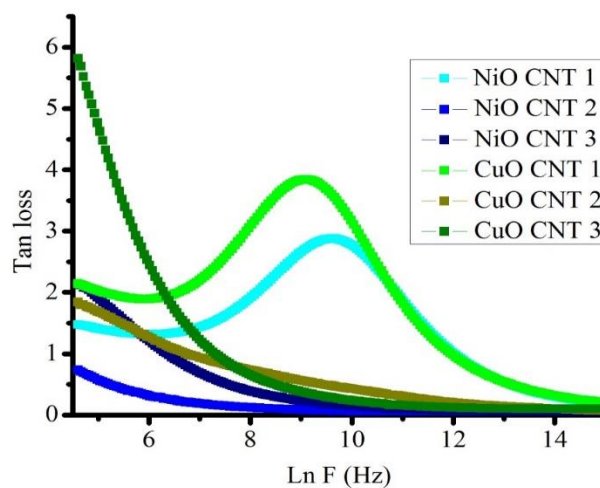
Figure 4.14. Tan loss measurement of all composites

hopping electrons resonanate with external electric field as shown in Fig 4.14 [111].Values observed in case of tan loss were low and no periodic trend was observed. AC conductivity of the material is its ability to allow the passage of current. When the external field is applied on

48

the material they allign themselves and their hopping frequency resonate with the external frequency it could be measured as [112]

$$\sigma_{ac} = 2\pi f \varepsilon' \varepsilon_o \tan\delta$$
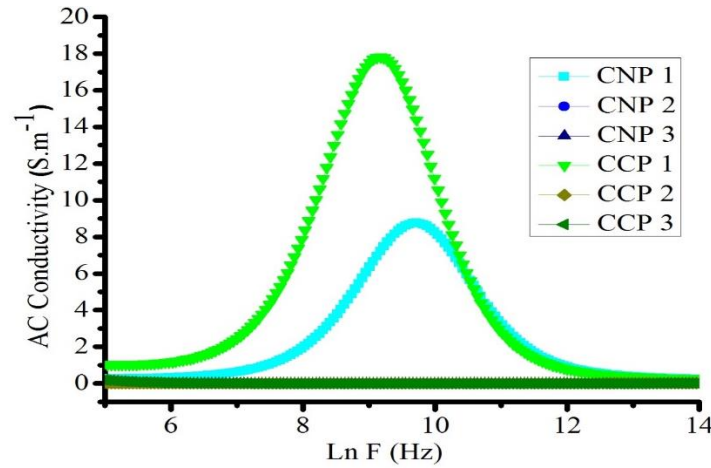
Figure 4.15. AC conductivity of all the composites

Fig 4.15. shows that CNP 1 and CCP 1 shows higher AC conductivity at low frequency as charge carrier easily allign themselves according to external applied field and it decreases as frequency increases as charge carrier did not get enough time to arrange themselves they move rendomly due to which AC conductivity decreases.

4.2.3. Mechanical Properties. Mechanical properties were investigated by using universal testing machine and drawing stress verses strain graph and different parameters like Yong's Modulus (E), Elastic limit (S_y), Ultimate tensile strength (UTS), Total strain (e_{total}), Elastic strain ($e_{elastic}$) and Toughness were calculated [113] [114]. The high brittleness of metal oxides was aimed to get control over the low toughness and high elasticity of polymer in addition to all these CNTs were employed to get enhanced mechanical properties. It was observed that by increasing metal oxide concentration, the toughness was enhanced and by adding CNT's elastic limit enhanced, variations in behavior were observed due migration of metal oxides and SWCNT's which require a more precise method to enhance mechanical strength more but still a good enhancement in mechanical parameters was observed.

By using similar stress vs strain graph mechanical properties of all the parameters were calculated as shown below in Table 4.2. It was seen that PVA has high elastic modulus and good elastic limit and by adding PVA in metal oxide their brittle nature was controlled by increasing concentration of metal oxide mechanical properties enhanced by further

49

incorporation of *f*-SWCNT's mechanical parameters shows enhanced elastic modulus, elastic limit and reduced value of strain produced as shown in Table 4.2.
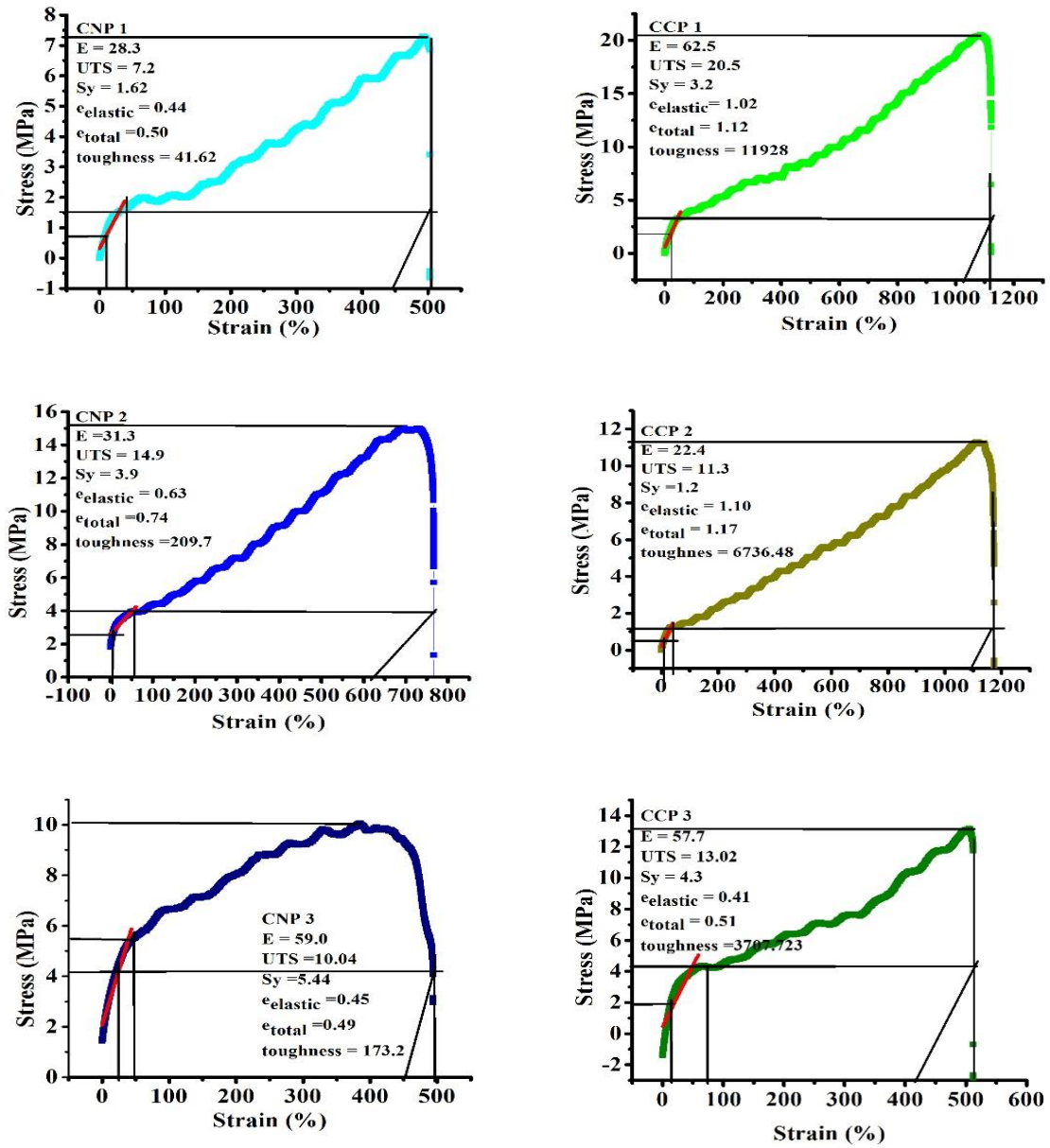
Figure 4.16. Mechanical properties analysis by stress strain graph

Table 4.1. Mechanical parameters of all the samples

Sr no	Sample	E (MPa)	S_y (MPa)	UTS (MPa)	e_{total}	$e_{elastic}$	Toughness/stiffness
1	PVA	71.5	34.4	95.4	0.37	0.32	24354.72
2	CNT 1	6.47	3.7	12.6	0.5	0.43	118.001
3	CN 2	7.8	4.1	9.2	0.335	0.25	2033.36
4	CN 3	13.15	8.87	23.4	0.720	0.614	399.10
5	CP 1	8.2	1.09	5.13	0.60	0.44	48.6
6	CP 2	18.9	0.37	1.7	0.62	0.53	652.77
7	CP 3	27.2	1.53	5.06	0.47	0.39	1445.26
8	NP 1	22.7	2.1	4.9	0.34	0.26	79.28
9	NP 2	25.7	1.6	2.5	0.26	0.13	62.2
10	NP 3	30.9	1.2	5.14	0.5	0.4	35.4
11	CCP 1	62.5	3.2	20.5	1.12	1.02	11928.18
12	CCP 2	22.4	1.2	11.3	1.17	1.10	6736.48
13	CCP 3	57.7	4.3	13.02	0.51	0.41	3707.723
14	CNP 1	28.3	1.62	7.2	0.50	0.44	41.62
15	CNP 2	31.3	3.9	14.9	0.74	0.63	209.7
16	CNP 3	59.0	5.44	10.04	0.49	0.45	173.2

Conclusions

For comparision detailed investigations have been carried out over pure PVA and composties in different combinations; PVA/MO, *f*-SWCNT/PVA and *f*-SWCNT/PVA/MO. In this course first of all 0.001 gm concenation of *f*- SWCNT's in PVA was optimized in order to maintain good transparancy with the help of UV-Vis studies. This optimized concentration of *f*-SWCNT was employed for further composite fabrication with varibale contents of nanoceramics; the NiO and CuO with crystallite sizes, 34.3 and 4.05 nm, respectively. Successful synthesis was confirmed with the help of FTIR, XRD, SEM and AFM techniques. In FTIR studies the functionalization of SWCNTs was confirmed due to appearance of –OH, -C=O, -So$_x$, -NO$_x$ and -C-H bands. FTIR analysis of Compoistes and *f*-SWCNT was observed the bnds at 2690 (-OH), 1788 (-C=O), 2136 (-NO$_X$, C-H stretch at 2136 cm-1 and 602 cm^{-1} (-SO$_X$) were observed in of *f*-SWCNT. It has also confirmed the synthesis of *f*-SWCNT/PVA/MO by appearance of individual peaks of all constituents. A peak shift was observed for NiO and CuO in XRPD patterns of *f*-SWCNT/PVA/MO along with the particular peak of *f*-SWCNT and a specific hump of PVA. SEM analysis reveald the homogeniety of *f*-SWCNT/PVA/MO composites along with the coild strucutre and ~40-80 nm diameter of *f*-SWCNT. AFM studies for 3-D images and topography under tapping mode confirmed the coiled structure of *f*-SWCNT inside the composites.

An increment of CuO concenteration led to decreases in band gap of PVA from 6.6 to 4.8, 4.7 and 4.5 eV for 0.01, 0.02, and 0.03 gm, respectively because of conductive pathways formation due to the arrangement of semiconductor CuO in polymer matrix. In case of when *f*-SWCNT/PVA/CuO band gap further reduced to 4.35, 4.30 and 4.20 eV due to semiconducting nature of coiled CNTs. Almost same trend was observed in case of PVA/NiO and SWCNT/PVA/CuO composites with band gap reduction range of 4.9 - 4.6 eV and 4.38 - 4.28 eV, respectively. Dielectric constant, dielectric loss, tan loss and AC-conductivity was evaluated and found that all these parameters could be controlled according to need by varying concentration of MO and SWCNT's. it was seen that the composites with least concentration of MO shows best current storing ability as in case of CCP1 value of dielectric constant, dielectric loss, tan loss and Ac conductivity was 3.3 x 10^7, 9.7 x10^8, 4.5 and 19 Sm^{-1} respectively and for CNP1 value of dielectric constant, dielectric loss, tan loss and Ac conductivity was 1.7 x 10^7, 3 x10^8, 2.5 and 9 Sm^{-1} respectively. The investigation of mechanical properties revealed the Young's modulus reduction of PVA from 71.2 to 6.47, 7.8 and 13.15 N/m for *f*-SWCNT/PVA composite with 0.001, 0.002 and 0.003 gm *f*-SWCNT concentrations,

respectively. For simple PVA/CuO values of Young's modulus were 8.2, 18.9 and 27.2 and were enhanced to 62.4, 22.5 and 57.7 N/m by addition of *f*-SWCNT's. Similarly for PVA/NiO values of Young's modulus were 22.7, 25.7, and 30.9 N/m by addition of *f*-SWCNT's enhanced to 28.3, 31.3 59.0 N/m. It was cuncluded that CCP1 and CCP2 show good mechanical strength, transmittance and dielectric properties and can be successfully used in supercapacitors.

References

[1]   G. WHITESIDES, J. MATHIAS, and C. SETO, "Molecular self-assembly and nanochemistry-A chemical strategy for the synthesis of nanostructures," *Science* **254**, 1312-1319, 1991.

[2]   G. A. Ozin, "Nanochemistry: synthesis in diminishing dimensions," *Advanced Materials,* **4**,612-649, 1992.

[3]   E. Llobet, "Gas sensors using carbon nanomaterials: A review," *Sensors and Actuators B: Chemical,* **179**, 32-45, 2013.

[4]   A. Alagarasi, "Introduction to Nanomaterials. 2013," *Unpublished).* http://www. *nccr. iitm. ac. in/2011.*

[5]   K. Scida, P. W. Stege, G. Haby, G. A. Messina, and C. D. García, "Recent applications of carbon-based nanomaterials in analytical chemistry: critical review," *Analytica chimica acta,* **691**, 6-17, 2011.

[6]   Q. Zhang, J. Q. Huang, W. Z. Qian, Y. Y. Zhang, and F. Wei, "The road for nanomaterials industry: A review of carbon nanotube production, post-treatment, and bulk applications for composites and energy storage," *Small,* **9**,1237-1265, 2013.

[7]   E. T. Thostenson, Z. Ren, and T.-W. Chou, "Advances in the science and technology of carbon nanotubes and their composites: a review," *Composites science and technology,* **61**, 1899-1912, 2001.

[8]   D. S. Hecht, L. Hu, and G. Irvin, "Emerging transparent electrodes based on thin films of carbon nanotubes, graphene, and metallic nanostructures," *Advanced materials,* **23**, 1482-1513, 2011.

[9]   L. Valentini, I. Armentano, J. Kenny, C. Cantalini, L. Lozzi, and S. Santucci, "Sensors for sub-ppm NO 2 gas detection based on carbon nanotube thin films," *Applied Physics Letters,* **82**, 961-963, 2003.

[10]   L. Hu, D. S. Hecht, and G. Gruner, "Carbon nanotube thin films: fabrication, properties, and applications," *Chemical reviews,* **110**, 5790-5844, 2010.

[11]   W. M. Doyle, "Principles and applications of Fourier transform infrared (FTIR) process analysis," *Process control and quality,* **2**, 11-41, 1992.

[12]   B. H. Stuart, *Infrared Spectroscopy: Fundamentals and Applications*: Wiley, 2004.

[13]   N. B. Colthup, L. H. Daly, and S. E. Wiberley, *Introduction to Infrared and Raman Spectroscopy*: Elsevier Science, 1990.

[14]   D. Stokes, *Principles and Practice of Variable Pressure: Environmental Scanning Electron Microscopy (VP-ESEM)*: Wiley, 2008.

[15]   B. C. Smith, *Fundamentals of Fourier Transform Infrared Spectroscopy, Second Edition*: CRC Press, 2011.

[16]   G. An, P. Yu, M. Xiao, Z. Liu, Z. Miao, K. Ding, *et al.*, "Low-temperature synthesis of Mn(3)O(4) nanoparticles loaded on multi-walled carbon nanotubes and their application in electrochemical capacitors," *Nanotechnology,* vol. **19**, 275709, 2008.

[17]

[18]   P. R. Griffiths, J. A. De Haseth, and J. D. Winefordner, *Fourier Transform Infrared Spectrometry*: Wiley, 2007.

[19]   M. Tasumi, *Introduction to Experimental Infrared Spectroscopy: Fundamentals and Practical Methods*: Wiley, 2014.

[20]   D. L. Pavia, G. M. Lampman, G. S. Kriz, and J. A. Vyvyan, *Introduction to Spectroscopy*: Cengage Learning, 2014.

[21]   D. McMullan, "Scanning electron microscopy 1928–1965," *Scanning,* **17**,. 175-185, 1995.

[22]   M. S. Kumar and A. Balaji, "Formulation amd evaluation of transformal gel of sumatriptan succinate

[23]   B. Lou, B. Peng, N. Rong, Y. Li, H. Chen, K. S. Sree, *et al.*, "Root and root endophytes from the eyes of an electron microscopist," in *Root Engineering*, ed: Springer, ,. 469-486. 2014

[24]   E. Suzuki, "High-resolution scanning electron microscopy of immunogold-labelled cells by the use of thin plasma coating of osmium," *Journal of Microscopy,* **208**, 153-157, 2002.

[25]   "<Dynamic_mechanical_behavior_of_melt-processed_mult.pdf>."

[26]   K. Tasneem, S.-H. Kim, J. Kim, B. H. Nam, and Y. Park, "Effects of Aggregate Mineralogy on the Thermal Expansion Behavior of Concrete," in *T&DI Congress 2014: Planes, Trains, and Automobiles* 163-172, 2014.

[27]   D. P. Diptonil Banerjee, "Synthesis of Amorphous Carbon Nanotube-copper hybrid and its optical properties" **4,2015.**

[28] J. S. Shaikh, R. C. Pawar, S. S. Mali, A. V. Moholkar, J. H. Kim, and P. S. Patil, "Effect of annealing on the supercapacitor performance of CuO-PAA/CNT films," *Journal of Solid State Electrochemistry,* **16**, 25-33, 2010.

[29] J. Goldstein, *Practical Scanning Electron Microscopy: Electron and Ion Microprobe Analysis*: Springer US, 2012.

[30] J. Goldstein, D. E. Newbury, D. C. Joy, C. E. Lyman, P. Echlin, E. Lifshin*, et al.*, *Scanning Electron Microscopy and X-ray Microanalysis: Third Edition*: Springer US, 2012.

[31] P. Echlin, *Handbook of Sample Preparation for Scanning Electron Microscopy and X-Ray Microanalysis*: Springer US, 2011.

[32] P. Echlin, C. E. Fiori, J. Goldstein, D. C. Joy, and D. E. Newbury, *Advanced Scanning Electron Microscopy and X-Ray Microanalysis*: Springer US, 2013.

[33] R. Zhou, C. Meng, F. Zhu, Q. Li, C. Liu, S. Fan*, et al.*, "High-performance supercapacitors using a nanoporous current collector made from super-aligned carbon nanotubes," *Nanotechnology,* vol. **21**, 345701, 2010.

[34] J. Tatami, T. Katashima, K. Komeya, T. Meguro, and T. Wakihara, "Electrically Conductive CNT-Dispersed Silicon Nitride Ceramics," *Journal of the American Ceramic Society,* **88**,2889-2893, 2005.

[35] K. E. Geckeler and H. Nishide, *Advanced Nanomaterials*: Wiley, 2009.

[36] J. R. Davis, *Tensile Testing, 2nd Edition*: ASM International, 2004.

[37] N. P. Khosla, K. I. Harikrishnan, N. C. D. o. T. Research, A. Group, and N. C. S. U. D. o. C. Engineering, *Tensile Strength: A Design and Evaluation Tool for Superpave Mixtures*: N.C. Department of Transportation, Research and Analysis Group, 2007.

[38] E. Flahaut, A. Peigney, C. Laurent, and A. Rousset, "Synthesis of single-walled carbon nanotube–Co–MgO composite powders and extraction of the nanotubes," *Journal of Materials Chemistry,* **10**,. 249-252, 2000.

[39] E. Flahaut, A. Peigney, C. Laurent, C. Marliere, F. Chastel, and A. Rousset, "Carbon nanotube–metal–oxide nanocomposites: microstructure, electrical conductivity and mechanical properties," *Acta Materialia,* **48**, 3803-3812, 2000.

[40] A. Peigney, E. Flahaut, C. Laurent, F. Chastel, and A. Rousset, "Aligned carbon nanotubes in ceramic-matrix nanocomposites prepared by high-temperature extrusion," *Chemical Physics Letters,* **352**, 20-25, 2002.

[41] J. Sun and L. Gao, "Development of a dispersion process for carbon nanotubes in ceramic matrix by heterocoagulation," *Carbon,* **41**, 1063-1068, 2003.

[42] Z. Guo-Dong, J. D. Kuntz, J. Wan, and A. K. Mukherjee, "Single-wall carbon nanotubes as attractive toughening agents in alumina-based nanocomposites," *Nature materials,* **2**, 38, 2003.

[43] M. Zhi, C. Xiang, J. Li, M. Li, and N. Wu, "Nanostructured carbon-metal oxide composite electrodes for supercapacitors: a review," *Nanoscale,* **5**, 72-88, 2013.

[44] S. Rul, F. Lefèvre-schlick, E. Capria, C. Laurent, and A. Peigney, "Percolation of single-walled carbon nanotubes in ceramic matrix nanocomposites," *Acta Materialia,* **52**, 1061-1067, 2004.

[45] X. Wang, N. P. Padture, and H. Tanaka, "Contact-damage-resistant ceramic/single-wall carbon nanotubes and ceramic/graphite composites," *Nat Mater,* **3** 539-44, 2004.

[46] E. L. Corral, J. Cesarano, A. Shyam, E. Lara-Curzio, N. Bell, J. Stuecker*, et al.*, "Engineered Nanostructures for Multifunctional Single-Walled Carbon Nanotube Reinforced Silicon Nitride Nanocomposites," *Journal of the American Ceramic Society,* **91**, 3129-3137, 2008.

[47] P.-C. Chen, G. Shen, Y. Shi, H. Chen, and C. Zhou, "Preparation and characterization of flexible asymmetric supercapacitors based on transition-metal-oxide nanowire/single-walled carbon nanotube hybrid thin-film electrodes," *ACS nano,* **4**,4403-4411, 2010.

[48] X. Zhang, W. Shi, J. Zhu, D. J. Kharistal, W. Zhao, B. S. Lalia*, et al.*, "High-power and high-energy-density flexible pseudocapacitor electrodes made from porous CuO nanobelts and single-walled carbon nanotubes," *ACS nano,* **5**, 2013-2019, 2011.

[49] A. C. Zaman, C. B. Üstündağ, F. Kaya, and C. Kaya, "OH and COOH functionalized single walled carbon nanotubes-reinforced alumina ceramic nanocomposites," *Ceramics International,* **38**, 1287-1293, 2012.

[50] D. Silambarasan, V. J. Surya, V. Vasu, and K. Iyakutti, "Single walled carbon nanotube-metal oxide nanocomposites for reversible and reproducible storage of hydrogen," *ACS Appl Mater Interfaces,* **5**, 11419-26, 2013.

[51] D. Silambarasan, V. J. Surya, V. Vasu, and K. Iyakutti, "One-step process of hydrogen storage in single walled carbon nanotubes-tin oxide nano composite," *International Journal of Hydrogen Energy,* **38**, 4011-4016, 2013.

[52]   B. Habibi, M. Jahanbakhshi, and M. Abazari, "A modified single-walled carbon nanotubes/carbon-ceramic electrode for simultaneous voltammetric determination of paracetamol and caffeine," *Journal of the Iranian Chemical Society,* **11**, 511-521, 2013.

[53]   R. Lavanya, V. J. Surya, I. Lakshmi, K. Iyakutti, V. Vasu, H. Mizuseki, *et al.*, "Hydrogen storage in TiO2 functionalized (10, 10) single walled carbon nanotube (SWCNT) – First principles study," *International Journal of Hydrogen Energy,* **39**,4973-4980, 2014.

[54]   M. Bocanegra-Bernal, C. Dominguez-Rios, J. Echeberria, A. Reyes-Rojas, A. Garcia-Reyes, and A. Aguilar-Elguezabal, "Spark plasma sintering of multi-, single/double-and single-walled carbon nanotube-reinforced alumina composites: Is it justifiable the effort to reinforce them?," *Ceramics International,* **42**, 2054-2062, 2016.

[55]   Y. Yao, G. Li, K. Gray, and R. M. Lueptow, "Titanium dioxide, single-walled carbon nanotube composites," ed: Google Patents, 2015.

[56]   A.-Y. Jee and M. Lee, "Comparative analysis on the nanoindentation of polymers using atomic force microscopy," *Polymer Testing,* **29**, 95-99, 2010.

[57]   M. K. Yew, H. Bin Mahmud, B. Ang, and M. Chian Yew, *Effects of Low Volume Fraction of Polyvinyl Alcohol Fibers on the Mechanical Properties of Oil Palm Shell Lightweight Concrete* 2015.

[58]   N. Tudorachi and R. D. Lipsa, *Poly(vinyl alcohol)-g-Lactic Acid Copolymers and Films with Silver Nanoparticles* **122**, 2011.

[59]   R. Bommulu and P. Pachamuthu, *Development of potentially biodegradable polyamide-6 and polyvinyl alcohol blends: Physico-mechanical properties, thermal properties, and soil test* **98**, 2005.

[60]   Z. Jin, K. Pramoda, G. Xu, and S. H. Goh, "Dynamic mechanical behavior of melt-processed multi-walled carbon nanotube/poly (methyl methacrylate) composites," *Chemical Physics Letters* **337**, 43-47, 2001.

[61]   D. Cai and M. Song, *Recent advance in functionalized graphene/polymer nanocomposites* **20**, 2010.

[62]   L. Deng, S. J. Eichhorn, C. C. Kao, and R. J. Young, "The effective Young's modulus of carbon nanotubes in composites," *ACS Appl Mater Interfaces,* **3**,433-40,2011.

[63]   N. T. B. Linh, K.-H. Lee, and B.-T. Lee, "Fabrication of photocatalytic PVA–TiO2 nano-fibrous hybrid membrane using the electro-spinning method," *Journal of Materials Science,* **46**, 5615-5620, 2011.

[64]   A. Sánchez Arribas, M. Moreno, M. Martínez-Fernández, E. Bermejo, A. Zapardiel, and M. Chicharro, "Effect of edge plane sites, oxygenated species and metallic impurities upon the electroactivity of carbon nanotube-modified electrodes toward hydrazine," *Sensors and Actuators B: Chemical,* **182**,31-39, 2013.

[65]   S. Barua, P. Chattopadhyay, M. M. Phukan, B. K. Konwar, and N. Karak, "Hyperbranched epoxy/MWCNT-CuO-nystatin nanocomposite as a high performance, biocompatible, antimicrobial material," *Materials Research Express,* **1**, 045402, 2014.

[66]   D. K. Singh, S. Mohan, V. Kumar, and S. H. Hasan, "Kinetic, isotherm and thermodynamic studies of adsorption behaviour of CNT/CuO nanocomposite for the removal of As (III) and As (V) from water," *RSC Advances,* **6**,1218-1230, 2016.

[67]   H. Huang, Y. Liu, J. Wang, M. Gao, X. Peng, and Z. Ye, "Self-assembly of mesoporous CuO nanosheets-CNT 3D-network composites for lithium-ion batteries," *Nanoscale,* **5**, 1785-8, 2013.

[68]   H. Hu, D. Zhang, Y. Liu, W. Yu, and T. Guo, "Highly enhanced field emission from CuO nanowire arrays by coating of carbon nanotube network films," *Vacuum,* **115**, 70-74, 2015.

[69]   S. Ko, J. I. Lee, H. S. Yang, S. Park, and U. Jeong, "Mesoporous CuO particles threaded with CNTs for high-performance lithium-ion battery anodes," *Adv Mater,* **24**, 4451-6, 2012.

[70]   C. Lee, S. H. Lee, M. Cho, and Y. Lee, "Nonenzymatic amperometric glucose sensor based on a composite prepared from CuO, reduced graphene oxide, and carbon nanotube," *Microchimica Acta,* vol. 183, pp. 3285-3292, 2016.

[71]   S. H. Park and W. J. Lee, "Hierarchically mesoporous CuO/carbon nanofiber coaxial shell-core nanowires for lithium ion batteries," *Sci Rep,* vol. 5, p. 9754, May 06 2015.

[72]   S. Mustansar Abbas, S. Tajammul Hussain, S. Ali, N. Ahmad, N. Ali, S. Abbas, *et al.*, "Modification of carbon nanotubes by CuO-doped NiO nanocomposite for use as an anode material for lithium-ion batteries," *Journal of Solid State Chemistry,* vol. 202, pp. 43-50, 2013.

[73]   S.-F. Zheng, J.-S. Hu, L.-S. Zhong, W.-G. Song, L.-J. Wan, and Y.-G. Guo, "Introducing dual functional CNT networks into CuO nanomicrospheres toward superior electrode materials for lithium-ion batteries," *Chemistry of Materials,* vol. 20, pp. 3617-3622, 2008.

[74]   A. D. Su, X. Zhang, A. Rinaldi, S. T. Nguyen, H. Liu, Z. Lei, *et al.*, "Hierarchical porous nickel oxide–carbon nanotubes as advanced pseudocapacitor materials for supercapacitors," *Chemical Physics Letters,* **561**, 68-73, 2013.

[75]   B. Nikahd and M. A. Khalilzadeh, "Liquid phase determination of bisphenol A in food samples using novel nanostructure ionic liquid modified sensor," *Journal of Molecular Liquids,* **215**, 253-257, 2016.

[76]   F. Su, X. Lv, and M. Miao, "High-performance two-ply yarn supercapacitors based on carbon nanotube yarns dotted with Co3 O4 and NiO nanoparticles," *Small,* **11**, 854-61, 2015.

[77]   G. S. Gund, D. P. Dubal, S. S. Shinde, and C. D. Lokhande, "Architectured morphologies of chemically prepared NiO/MWCNTs nanohybrid thin films for high performance supercapacitors," *ACS applied materials & interfaces,* **6**, 3176-3188, 2014.

[78]   H.-Y. Chang, H.-C. Chang, and K.-Y. Lee, "Characteristics of NiO coating on carbon nanotubes for electric double layer capacitor application," *Vacuum,* **87**,164-168, 2013.

[79]   M. Jayalakshmi and K. Balasubramanian, "Simple capacitors to supercapacitors-an overview," *Int. J. Electrochem. Sci,* **3**, 1196-1217, 2008.

[80]   J. Y. Lee, K. Liang, K. H. An, and Y. H. Lee, "Nickel oxide/carbon nanotubes nanocomposite for electrochemical capacitance," *Synthetic metals,* **150**, 153-157, 2005.

[81]   J. Huang, N. Zhu, T. Yang, T. Zhang, P. Wu, and Z. Dang, "Nickel oxide and carbon nanotube composite (NiO/CNT) as a novel cathode non-precious metal catalyst in microbial fuel cells," *Biosensors and Bioelectronics,* **72**, 332-339, 2015.

[82]   M. S. Wu, Y. R. Zheng, and G. W. Lin, "Three-dimensional carbon nanotube networks with a supported nickel oxide nanonet for high-performance supercapacitors," *Chem Commun (Camb),* **50**, 8246-8, 2014.

[83]   M. Fouladgar, "A new sensor for determination of nalbuphine using NiO/functional single walled carbon nanotubes nanocomposite and ionic liquid," *Sensors and Actuators B: Chemical,* **230**, 456-462, 2016.

[84]   M. Gong, W. Zhou, M. C. Tsai, J. Zhou, M. Guan, M. C. Lin, *et al.*, "Nanoscale nickel oxide/nickel heterostructures for active hydrogen evolution electrocatalysis," *Nat Commun,* **5**,4695, 2014.

[85]   M. Hong, H. C. Choi, and H. R. Byon, "Nanoporous NiO Plates with a Unique Role for Promoted Oxidation of Carbonate and Carboxylate Species in the Li–O2Battery," *Chemistry of Materials,* **27**, 2234-2241, 2015.

[86]   N. I. Andersen, A. Serov, and P. Atanassov, "Metal oxides/CNT nano-composite catalysts for oxygen reduction/oxygen evolution in alkaline media," *Applied Catalysis B: Environmental,* **163**, 623-627, 2015.

[87]   P. Lin, Q. She, B. Hong, X. Liu, Y. Shi, Z. Shi, *et al.*, "The nickel oxide/CNT composites with high capacitance for supercapacitor," *Journal of The Electrochemical Society,* **157**, A818-A823, 2010.

[88]   Z. Ruifeng, M. Chuizhou, Z. Feng, L. Qunqing, L. Changhong, F. Shoushan, *et al.*, "High-performance supercapacitors using a nanoporous current collector made from super-aligned carbon nanotubes," *Nanotechnology,* vol. 21, p. 345701, 2010.

[89]   S. Mustansar Abbas, S. Tajammul Hussain, S. Ali, K. Shahzad Munawar, N. Ahmad, and N. Ali, "Facile synthesis of carbon nanotubes supported NiO nanocomposite and its high performance as lithium-ion battery anode," *Materials Letters,* vol. 107, pp. 158-161, 2013/09/15/ 2013.

[90]   N. Duraisamy, A. Numan, S. O. Fatin, K. Ramesh, and S. Ramesh, "Facile sonochemical synthesis of nanostructured NiO with different particle sizes and its electrochemical properties for supercapacitor application," *J Colloid Interface Sci,* **471**,136-144, 2016.

[91]   J. Zhu, D. Li, H. Chen, X. Yang, L. Lu, and X. Wang, "Highly dispersed CuO nanoparticles prepared by a novel quick-precipitation method," *Materials Letters,* **58**,3324-3327, 2004.

[92]   C.-C. CIOBOTARU, C. M. DAMIAN, and H. IOVU, "Single-wall carbon nanotubes purification and oxidation," *UPB Sci. Bull., Series B,* **75**,55-66, 2013.

[93]   A. Rinzler, J. Liu, H. Dai, P. Nikolaev, C. Huffman, F. Rodriguez-Macias, *et al.*, "Large-scale purification of single-wall carbon nanotubes: process, product, and characterization," *Applied Physics A: Materials Science & Processing,* **67**, 29-37, 1998.

[94]   G. Socrates, *Infrared and Raman characteristic group frequencies: tables and charts*: John Wiley & Sons, 2001.

[95]   A. Maltsev, T. Bally, M.-L. Tsao, M. S. Platz, A. Kuhn, M. Vosswinkel, *et al.*, "The rearrangements of naphthylnitrenes: UV/Vis and IR spectra of azirines, cyclic ketenimines, and cyclic nitrile ylides," *Journal of the American Chemical Society,* **126**, 237-249, 2004.

[96]   B. B. Doyle, E. Bendit, and E. R. Blout, "Infrared spectroscopy of collagen and collagen-like polypeptides," *Biopolymers,* **14**, 937-957, 1975.

[97]   F. Davar, Z. Fereshteh, and M. Salavati-Niasari, "Nanoparticles Ni and NiO: synthesis, characterization and magnetic properties," *Journal of Alloys and Compounds,* **476**, 797-801, 2009.

[98]   H. S. Mansur, C. M. Sadahira, A. N. Souza, and A. A. Mansur, "FTIR spectroscopy characterization of poly (vinyl alcohol) hydrogel with different hydrolysis degree and chemically crosslinked with glutaraldehyde," *Materials Science and Engineering: C,* vol. **28**, 539-548, 2008.

[99]   N. Kouklin, M. Tzolov, D. Straus, A. Yin, and J. Xu, "Infrared absorption properties of carbon nanotubes synthesized by chemical vapor deposition," *Applied Physics Letters,* **85,** 4463-4465, 2004.

[100]   T. Heitz, B. Drévillon, C. Godet, and J. E. Bourée, "Quantitative study of C\char22{}H bonding in polymerlike amorphous carbon films using in situ infrared ellipsometry," *Physical Review B,* **58**, 13957-13973, 1998.

[101]   T. A. Saleh, "The role of carbon nanotubes in enhancement of photocatalysis," in *Syntheses and Applications of Carbon Nanotubes and Their Composites*, ed: InTech, 2013.

[102]   Q. A. Acton, *Advances in Carbon Research and Application,* 2012.

[103]   D. Liu, J. Li, F. Sun, R. Xiao, Y. Guo, and J. Song, "Liquid crystal microphase separation of cellulose nanocrystals in wet-spun PVA composite fibers," *RSC Advances,* **4,**30784-30789, 2014.

[104]   H. Siddiqui, M. Qureshi, and F. Z. Haque, "Surfactant assisted wet chemical synthesis of copper oxide (CuO) nanostructures and their spectroscopic analysis," *Optik-International Journal for Light and Electron Optics,* **127**,2740-2747, 2016.

[105]   A. A. Christy, O. M. Kvalheim, and R. A. Velapoldi, "Quantitative analysis in diffuse reflectance spectrometry: a modified Kubelka-Munk equation," *Vibrational Spectroscopy,* **9**, 19-27, 1995.

[106]   L. Yang and B. Kruse, "Revised Kubelka–Munk theory. I. Theory and application," *JOSA A,* **21**,1933-1941, 2004.

[107]   O. G. Abdullah, S. B. Aziz, K. M. Omer, and Y. M. Salih, "Reducing the optical band gap of polyvinyl alcohol (PVA) based nanocomposite," *Journal of Materials Science: Materials in Electronics,* **26**,5303-5309, 2015.

[108]   E. S. Goh, T. Chen, C. Sun, and Y. Liu, "Thickness effect on the band gap and optical properties of germanium thin films," *Journal of applied physics,* **107**,024305, 2010.

[109]   I. Gul and A. Maqsood, "Structural, magnetic and electrical properties of cobalt ferrites prepared by the sol–gel route," *Journal of Alloys and Compounds,* **465**, 227-231, 2008.

[110]   J. K. Rao, A. Raizada, D. Ganguly, M. M. Mankad, S. Satayanarayana, and G. Madhu, "Investigation of structural and electrical properties of novel CuO–PVA nanocomposite films," *Journal of materials science,* **50**, 7064-7074, 2015.

[111]   A. Azam, A. S. Ahmed, M. S. Ansari, and A. H. Naqvi, "Study of electrical properties of nickel doped SnO 2 ceramic nanoparticles," *Journal of Alloys and Compounds,* **506**, 237-242, 2010.

[112]   H. El-Mallah, "AC electrical conductivity and dielectric properties of perovskite (Pb, Ca) TiO3 ceramic," *Acta Physica Polonica-Series A General Physics,* **122,**174, 2012.

[113]   S. Popovics, "A numerical approach to the complete stress-strain curve of concrete," *Cement and concrete research,* **3**, 583-599, 1973.

[114]   T. T. Hsu, F. O. Slate, G. M. Sturman, and G. Winter, "Microcracking of plain concrete and the shape of the stress-strain curve," in *Journal Proceedings*, 209-224, 1963.